Study of Block Onset Using Sensitivity Perturbations in Climatological Flows

ZHIJIN LI

Supercomputer Computations Research Institute, The Florida State University, Tallahassee, Florida

ALBERT BARCILON

Department of Meteorology and Geophysical Fluid Dynamics Institute, The Florida State University, Tallahassee, Florida

I. M. NAVON

Department of Mathematics and Supercomputer Computations Research Institute, The Florida State University, Tallahassee, Florida

(Manuscript received 5 February 1998, in final form 2 June 1998)

ABSTRACT

This work describes the dynamics of adjoint sensitivity perturbations that excite block onsets over the Pacific and Atlantic Oceans. Appropriate functions are derived for the blocking indices for these two regions and the model basic flow is constructed from Northern Hemisphere climatological data. The concepts of sensitivity analysis are extended to forced problems. This tool is used to investigate block onset due to atmospheric forcing, such as that resulting from tropical sea surface temperature anomalies. These linear studies are carried out in a hemispherical, primitive equations, θ-coordinate, two-layer model.

Results show that wind sensitivity perturbations less than 10 m s^{-1} and sensitivity forcing of vorticity sources of the order of 1.5×10^{-10} s^{-2} are sufficient to excite block onset. Both for the Pacific and Atlantic blocking, sensitivity perturbations and forcing perturbations, when expressed in terms of vertical vorticity, display a Rossby wave train structure mainly found on the southward flanks of the Pacific and Atlantic jets, that is, near the Philippines and the Caribbean regions.

From inferences based on the flow evolution of these sensitivity perturbations and with the help of potential vorticity analyses on the two constant potential temperature surfaces in this model, a dynamical framework that may explain Pacific and Atlantic block onsets is proposed. The nonuniform potential vorticity distribution in the jets, in particular the concentration of these gradients on potential vorticity waveguides, and the Lagrangian advection of potential vorticity by the eddies making up the stationary Rossby wave train and their energy propagation and convergence all conspire to play a key role in the growth of the synoptic-scale eddies supported by baroclinic as well as barotropic processes. It is proposed that the structural modification of the eddies in the wave train leads to the planetary structures that become associated with block onset. More specifically, the wave train in the Pacific evolves into a blocking dipole while the Atlantic block is found at the leading edge of the Rossby wave train across the Atlantic. Furthermore, this study shows that at the initial time the Pacific block displays a clear baroclinic structure while the wave train associated with the Atlantic block has a much more barotropic structure.

The significance of these results and their potential applications to predictions of blocking are discussed.

1. Introduction

A blocking flow configuration frequently causes lasting anomalous weather situations over large extratropical regions. Forecasting the onset of blocks is still a difficult task even for up-to-date models (Tibaldi and Molteni 1990; Kimoto et al. 1992; Anderson 1993; Tibaldi et al. 1994). A large number of the unskilled forecasts can be traced to the model's inability to predict block onset beyond a few days into the forecast due to the increased sensitivity of the model atmosphere to small changes in the dynamics (Lorenz 1965). Understanding the dynamics of blocking is an important step toward improved medium- and long-range forecasting.

Identification of precursors of block onset may enhance the prediction of blocking and many studies have searched for such precursors. For example, observational studies by Lejenäs and Madden (1992) and Hansen and Sutera (1993) suggested that large-amplitude planetary waves are present in about a third of the block onsets and argued for planetary waves as precursors of

Corresponding author address: Prof I. M. Navon, Department of Mathematics, Supercomputer Computations Research Institute, The Florida State University, Tallahassee, FL 32306-4130.
E-mail: navon@scri.fsu.edu

block onset. Yet, from his case study of blocking, Bengtsson (1981) concluded that in this particular case the amplitude of the ultralong waves were reduced by as much as 40% during the buildup of the blocking pattern. Kushnir (1987) and Plaut and Vautard (1994) suggested that block onset is linked to a particular phase of the Branstator–Kushnir 20–25-day low-frequency oscillations (Branstator 1987). Colucci and Alberta (1996) compiled statistics on case studies of block onsets in the Atlantic and Pacific for seven winters. They listed five possible precursors involving intensity and direction of the horizontal wind and its anomaly and the explosive development of a surface cyclone properly positioned with respect to the location where the block forms. They argued that block onset cyclones each coincided with a cyclonic–anticyclonic couplet in the synoptic quasigeostrophic (QG) potential vorticity (PV) field at 500 mb. Low-frequency and/or planetary-scale dynamics may be instrumental in block onset, but they do not operate in every blocking event. This may be a reflection of multiplicity of blocking mechanisms.

A central question dealing with the role of synoptic eddies in block onset is, How do the transient eddies organize a blocking structure? One answer to that question postulates a statistical aggregate effect of these eddies leading to block onset (e.g., Shutts 1986). Another views block onset as an evolutionary process in which a subset of synoptic eddies become the blocking structure in a few days. For reasons discussed below, this work favors this last picture.

The role of the synoptic eddies in the onset phase of blocks and of larger-scale anomalies is not clear. Observational studies seem to suggest that Pacific block onsets are much more affected by the transient high-frequency eddies while the Atlantic block onsets are much more susceptible to the convergence of the wave activity flux density associated with the low-frequency eddies, that is, eddies with timescales exceeding one week (Nakamura et al. 1997). Studies of the rapid formation of a blocking episode following the occurrence of strong cyclogenesis upstream (e.g., Colucci 1985, 1987; Crum and Stevens 1988; Konrad and Colucci 1988) have suggested that intense synoptic-scale eddies may play an important role in block onset. Some observational studies have found evidence of enhanced synoptic activity upstream of a developing block (Dole 1986, 1989; Nakamura and Wallace 1990), the enhanced synoptic variability propagating downstream and becoming incorporated into the block. The genesis of these large-scale anomalies may be rooted in baroclinic–barotropic instabilities of a three-dimensional flow (Frederiksen 1983; Frederiksen and Bell 1990). Other studies proposed that the mechanism associated with anomalous PV transports by synoptic-scale eddies (Shutts 1986; Tsou and Smith 1990) may be responsible for the rapid development of these large-scale flow anomalies. Higgins and Schubert (1994) found that, just before onset of the Pacific positive anomalies, the pattern of anomalous synoptic-scale eddy activity organized into a large-scale east–west band over the western Pacific and eastern Asia.

By constructing block composites, Nakamura and Wallace (1993) studied the role of synoptic-scale eddies during block onset. They, as well as other authors, found that in all cases advection of PV played an important part in these onsets. Furthermore, one or two migratory cyclones and anticyclones appeared to be associated with the onset of the block pattern.

Black and Dole (1993) described the evolution of persistent Pacific anomalies in terms of a two-stage life cycle. In the first stage, transient propagating eddies are found while quasi-stationary, but growing, eddies are present in the second stage. Black and Dole conjectured that the first stage was due to nonmodal growth and argued that the source of energy for that stage is *local* and resides in the shears associated with the background flow. They surmised that the second stage was due to the growth of the most unstable normal mode of a three-dimensional climatological flow (Frederiksen 1983).

Pondeca et al. (1998b) analyzed four model blocking events: one of the blocks was present in the control run, while the other three were excited by sensitivity perturbations added at a judicious time on flows characterized as zonal by the blocking index. The events leading to block onset were quite similar in all four cases, and block onset consisted of two phases. The first, which displayed the formation of cutoff cyclones in the upper layer, was characterized by nonmodal growth in which baroclinic and barotropic processes cooperated. The second phase was characterized by an intense instability of normal-mode form with mechanisms similar to the ones described by Frederiksen and Bell (1990). This life cycle leading to block onset has a number of common features with that of Black and Dole (1993).

From observational evidence in classical blocking studies (e.g., Rex 1950) and in more recent composite studies of block onset (e.g., Nakamura and Wallace 1993; Nakamura 1994; Nakamura et al. 1997) as well as anomaly onsets studies discussed above, we conjecture that the nonmodal growth of a set of synoptic-scale eddies may be responsible for the development of the planetary-scale, blocking dipole or the blocking anticyclone. Inasmuch as nonmodal growth typically involves cooperating barotropic and baroclinic processes, this conjecture is supported by data analysis over the Pacific region (Black and Dole 1993). Recently, Barcilon and Bishop (1998) considered the evolution of a baroclinic wave in the presence of horizontal shear described in terms of nonmodal disturbances. They found that that perturbation is capable of drawing energy simultaneously from the basic-state momentum and temperature gradients.

This study, then, deals with the structural changes associated with perturbations initially possessing synoptic scales as they directly evolve into the blocking structure. We use sensitivity analysis in conjunction with

blocking indices and model flows derived from the Northern Hemisphere climatology. As our initial perturbation, we use the ''sensitivity perturbation.'' Because of its alignment with the blocking index gradient, the sensitivity perturbation produces the largest possible changes in the blocking index.

We extend the concept of sensitivity perturbation to a time-dependent, forced problem in which the initial perturbation is assumed to be zero. We designate that perturbation as ''forcing perturbation.'' We use this tool to understand block onset resulting from forcing as associated with secondary atmospheric circulations. An example of these circulations may be those associated with tropical sea surface temperature (SST) anomalies (e.g., Ferranti et al. 1994).

We qualitatively analyze the evolution of sensitivity perturbations by focusing on their PV dynamics on the two constant potential temperature levels in our model. From these analyses emerges a physical picture of Pacific and Atlantic block onsets. In the dynamical picture we offer, the sensitivity perturbation, the background PV gradients associated with the jets and the Tropics, the Rossby wave packet and its eddies, the Lagrangian advection of PV by the eddies, and the mechanisms of energy propagation and convergence all conspire to take part in the orchestration of block onset, which occurs in two stages. In the first stage, the leading wave packet cyclonic eddy builds up. In the second stage, the low PV advection by this eddy, as well as the energy convergence, produce the blocking anticyclone. This qualitative discussion of the various events taking part in the evolution toward block onset as well as their mechanisms provides a dynamical framework in which to explain recent composite observations of block onset (Nakamura 1994; Nakamura et al. 1997; Michelangeli and Vautard 1998), and to test new theories.

The outline of this paper is as follows. In section 2, we summarize the features of the model and briefly discuss the adjoint sensitivity methods. Section 3 presents the results of adjoint sensitivity analysis and the evolution of sensitivity perturbations in the presence of the climatological flow derived from Northern Hemisphere atmospheric data (1984–93). This section describes sensitivity studies over the Pacific and Atlantic Oceans. Section 4 deals with the sensitivity forcing for Pacific and Atlantic blocks. Section 5 discusses the results of this study.

2. Model description and sensitivity analysis

We summarize below the properties of the numerical model and outline the mathematics associated with sensitivity analysis.

a. Model description

The hemispherical two-layer isentropic primitive equation model described in the appendix of Zou et al. (1993) is used in this study. The predictive equations are written for the spherical harmonic coefficients of the isentropic vorticity ζ, the divergence D, and the Exner-layer thickness $\Delta\pi$. The spherical harmonic expansion is truncated at T31. The vertical discrete analog of the model equations and relevant model parameters are given in the appendix. In the present study, only its linearized dynamics is used.

We generically write the nonlinear model dynamics in terms of its time-dependent spectral coefficients as

$$\frac{dx}{dt} = N(x) + F, \tag{2.1}$$

where x is the state vector consisting of the real spectral coefficients of ζ, D, and $\Delta\pi$ for the two layers. The vector F is an appropriate forcing function, which we introduce and discuss in the appendix. This function will be used only in the sensitivity forcing section. After we linearize (2.1), the evolution of the perturbation δx of the state vector x is governed by the tangent linear plane dynamics,

$$\frac{d}{dt}\delta x = L\delta x + \delta F, \tag{2.2}$$

where L is the Jacobian matrix of N evaluated on the trajectory $x(t)$ and δF is the perturbation to the forcing function F.

b. Response function

A sensitivity perturbation is determined by the gradient of a selected response function (Rabier et al. 1996) appropriate to the problem considered. In this problem, the response function is a blocking index. There are several expressions of blocking indices in the literature (Rex 1950; Lejenäs and Okland 1983; Liu 1994; Liu and Opsteegh 1995) and we select the blocking index proposed by Liu (1994):

$$R(x) = \langle x - x_c, x_b\rangle/\langle x_b, x_b\rangle, \tag{2.3}$$

where

$$\langle x_1, x_2\rangle = \int_\Omega x_1 x_2 \, d\Omega \tag{2.4}$$

defines the inner product, Ω represents the area of the hemisphere, x_c is the climatological state vector, and x_b represents the blocking spatial anomaly pattern. The response function $R(x)$ is then the normalized projection of flow anomalies on the blocking anomaly pattern. This form of blocking index was used in sensitivity analysis studies by Oortwijn and Barkmeijer (1995), Oortwijn (1998), and Pondeca et al. (1998a,b).

c. Sensitivity to changes in initial conditions

In an inner product space, a defined function $R(x)$ satisfies

$$\delta R = (\nabla_x R, \delta x), \tag{2.5}$$

where (,) denotes an inner product and $\nabla_x R$ is the gradient of R with respect to x (e.g., Talagrand and Courtier 1987).

Taking the variation of (2.3) with respect to x, we obtain

$$\delta R = \langle \delta x(t), x_b \rangle / \langle x_b, x_b \rangle. \tag{2.6}$$

When the forcing is not taken into account, that is, $F = \delta F = 0$, we integrate the linear equation (2.2) from t_0 to t and write its solution as

$$\delta x(t) = \mathbf{A}(t, t_0)\delta x(t_0), \tag{2.7}$$

where $A(t, t_0)$ is the resolvent. We substitute (2.7) into (2.6) and make use of the definition of an adjoint operator and get

$$\begin{aligned} \delta R &= \langle \mathbf{A}(t, t_0)\delta x(t_0), x_b \rangle / \langle x_b, x_b \rangle \\ &= \langle \delta x(t_0), \mathbf{A}^{\mathrm{T}}(t, t_0)x_b \rangle / \langle x_b, x_b \rangle. \end{aligned} \tag{2.8}$$

The superscript ''T'' denotes the transpose. Since $\mathbf{A}$ is a real matrix, $\mathbf{A}^{\mathrm{T}}$ is the adjoint operator of $\mathbf{A}$.

Comparing (2.8) with (2.5), we immediately obtain the gradient of the response function $R(x)$ with respect to the initial condition $x(t_0)$:

$$\nabla_{x(t_0)} R = \mathbf{A}^{\mathrm{T}}(t, t_0)x_b / \langle x_b, x_b \rangle. \tag{2.9}$$

Because the adjoint of the resolvent for integrations from t_0 to t is equal to the resolvent of the adjoint from t to t_0 (Talagrand and Courtier 1987), it follows that (2.9) can be solved by a single integration of the adjoint model, that is, by a backward integration of the adjoint model from t to t_0, starting from the final condition $x_b / \langle x_b, x_b \rangle$.

From (2.8) and (2.9), we infer that the change in the blocking index is maximum when the initial perturbation δx_0 is parallel to its respective gradient. We use an appropriately scaled gradient field as the initial perturbation that we denote as the sensitivity initial perturbation or, for short, *sensitivity perturbation.*

The model state vector x consists of spectral coefficients of vorticity, divergence, and Exner-layer thickness, but we may calculate the sensitivity of the blocking index to another state vector y such that $x = \mathbf{C}y$. The gradient of R with respect to $y(t_0)$ is

$$\nabla_{y(t_0)} R = \mathbf{C}^{\mathrm{T}} \nabla_{x(t_0)} R. \tag{2.10}$$

Equation (2.10) follows immediately from (2.8) by writing $\delta x(t_0) = \mathbf{C}\delta y(t_0)$ and using the definition of an adjoint operator. Here $\mathbf{C}$ is constant matrix. Note that the R-sensitivity to y is *not* $\mathbf{C}^{-1}\nabla_{x(t_0)} R$.

In the present study, the R-sensitivity is calculated only with respect to $x(t_0)$ made up of the wind components and the Exner-layer thickness. By trial and error, we found that sensitivity perturbations with respect to the state vector consisting of vorticity and divergence or streamfunction and velocity potential function did not evolve into typical blocking patterns. This is because the constant matrix $\mathbf{C}$, which relates the x and y vectors, depends upon the choice of the dependent function making up these vectors. The elements of $\mathbf{C}$ strongly depend upon horizontal wavenumbers in this case. As a result, the sensitivity perturbation calculated with respect to vorticity and divergence has scales too large to excite block onset, whereas the sensitivity perturbation calculated with respect to streamfunction (Zou et al. 1993; Frederiksen 1997) and velocity potential has scales too small to excite block onset.

3. Results of sensitivity analyses

The climatological time-mean flow possesses realistic three-dimensional features associated with atmospheric dynamics. It can be viewed as a dynamical equilibrium state not far from the actual atmospheric state especially if the time over which the average is performed is from two to four weeks. Several studies have used climatological flows as their background flow: to wit, the study of normal modes (e.g., Simmons et al. 1983; Frederiksen 1982), optimal perturbations (e.g., Borges and Hartmann 1992), optimally forced perturbations (Li and Ji 1997), as well as studies pertaining to the propagation of a perturbation (e.g., Hoskins and Ambrizzi 1993).

The model basic flow is constructed from 10 yr of mean monthly January data of the National Aeronautics and Space Administration (NASA) Data Assimilation Office (DAO) from 1984 to 1993. With the use of a cubic spline, we interpolate the data from pressure surfaces in the data to the model potential temperature surfaces selected as 306 and 330 K for the lower and upper surfaces, respectively. These surfaces roughly corresponded to 700 and 250 hPa at middle latitudes. When superadiabatic lapse rates were encountered in the data, we ignored these values and replaced them with the mean of the nearest six grid values, which had no superadiabatic lapse rates.

We use ''PV thinking'' to understand the dynamics of block onset (Hoskins et al. 1985; Crum and Stevens 1988) and analyze the PV on isentropic surfaces (IPV), where, in the kth layer of the model, the IPV is given by

$$P_k = Rg\pi_k \Delta\theta(f + \zeta_\theta)/C_p p_k \Delta\pi_k \qquad k = 1, 2. \tag{3.1}$$

In the above expression, $p_k = p_0(\pi_k/C_p)^{C_p/R}$, ζ_θ is the vertical component of relative vorticity on the θ surface, f is the Coriolis parameter, and the other symbols have their standard meaning.

Figure 1 displays contours of constant zonal wind on the two θ-surfaces of the model as derived from the January climatology. Figure 2 shows the climatological IPV on the two model θ-surfaces. As seen in these figures, in these two model layers the main features of the Pacific and Atlantic jets are reasonably represented. These jets, especially the Pacific jet, contain strong horizontal and vertical shears. The model is expected to adequately describe barotropic and baroclinic processes.

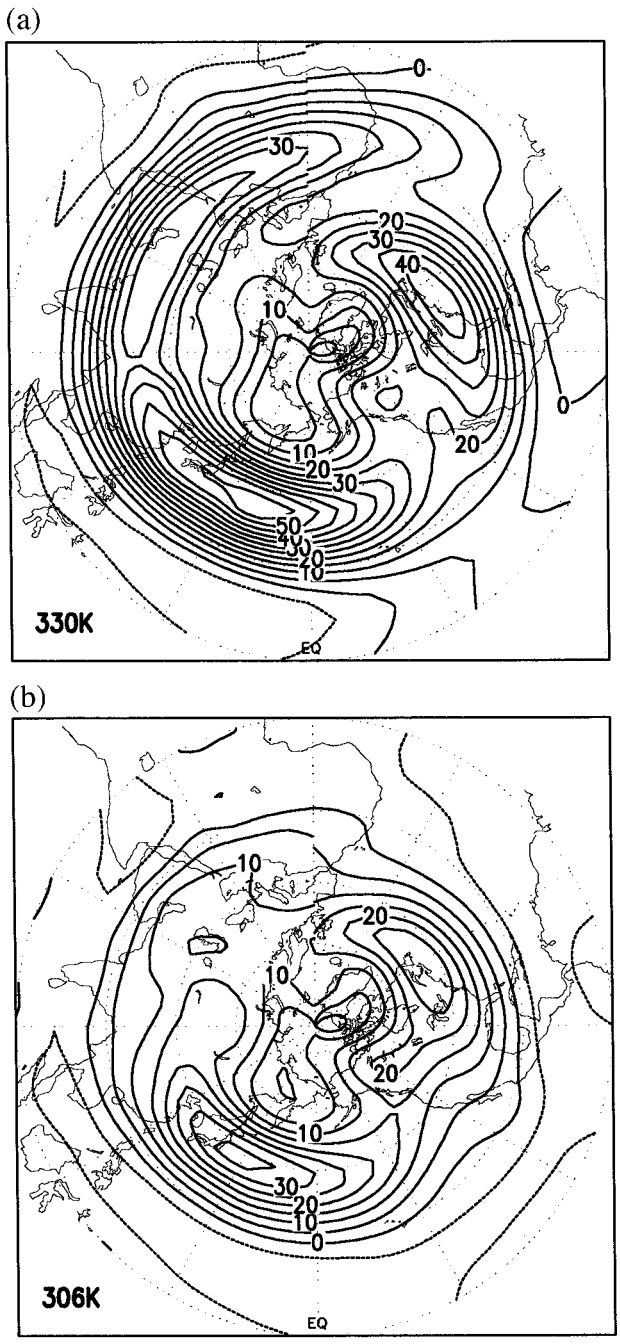

FIG. 1. The basic state used in the two-layer isentropic model. (a) Climatological mean zonal wind component from 10 yr of mean monthly January 1984–93 NASA analyses at 330 K; (b) at 306 K. The contour interval is 5 m s^{-1}. The outmost latitude circle (EQ) is the equator.

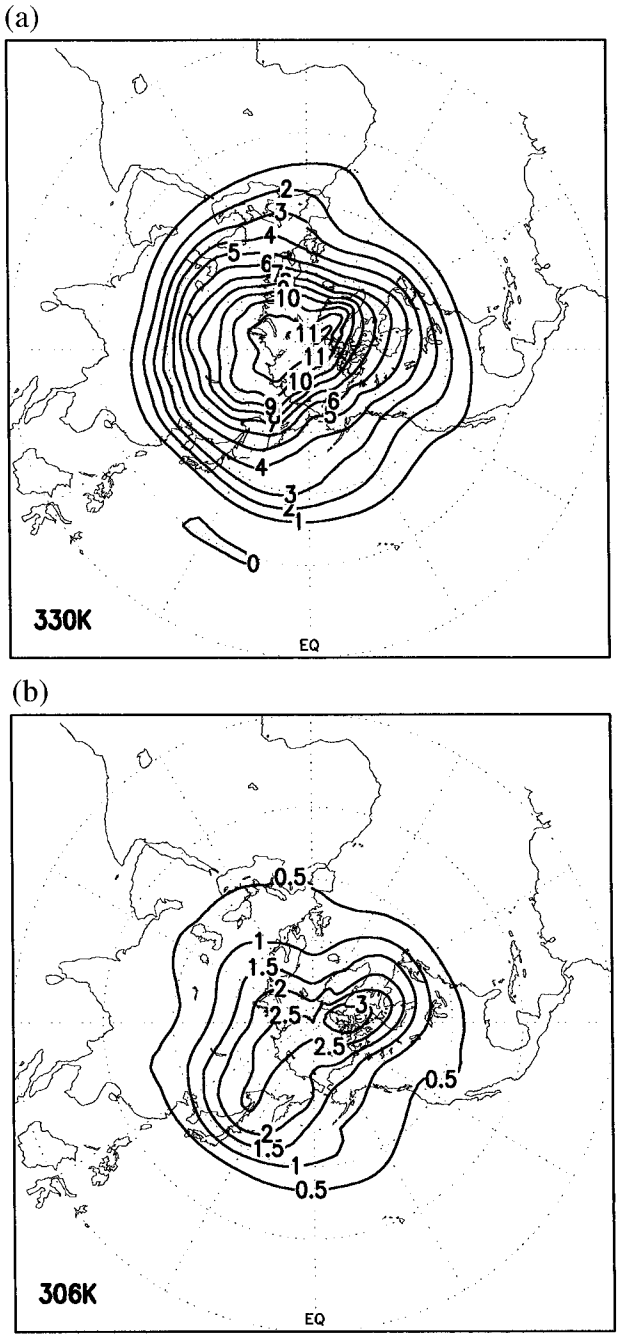

FIG. 2. Climatological mean isentropic potential vorticity (IPV) (a) at 330 K, the contour interval is 1 PV unit; (b) at 306 K, the contour interval is 0.5 PV unit. 1 PV unit is 10^{-6} m^2 s^{-1} K kg^{-1}.

From the composite analysis of say, Nakamura et al. (1997), blocking anticyclones are preferentially located northeast of the jet exits. The Pacific and Atlantic blocking areas are located in the weak, low IPV troughs.

Below, we carry out sensitivity analyses for the Pacific and Atlantic blocks. From the block composites presented by Nakamura et al. (1997, see their Figs. 1 and 2), the Pacific blocks seem to be centered close to 56°N, 165°W, and the Atlantic blocks seem to be centered close to 54°N, 10°E. In the choice of the response function (2.3), we assume that the pattern x_b depends only on the streamfunction, ψ_b (e.g., Zou et al. 1993). We argue that the shape of the block signature will depend on a few parameters. Assuming such a shape to

be elliptical-like, then the north–south extent (minor axis) and the east–west extent (major axis) are the most important parameters. Assuming a barotropic structure, we represent such a shape by a simple analytical expression based on observations (Nakamura et al. 1997) to construct ψ_b:

$$\psi_b = \overline{\psi_b}\left\{\left[1 - \cos\left(\frac{\lambda - \lambda_w}{\lambda_E - \lambda_w}\pi\right)\right] \times \left[1 - \cos\left(\frac{\phi - \phi_S}{\phi_N - \phi_S}\pi\right)\right]\right\}^{\alpha}, \quad (3.2)$$

for $\lambda_W < \lambda < \lambda_E$, $\phi_S < \phi < \phi_N$, otherwise $\psi_b = 0$. Here λ is longitude and ϕ latitude. For the Pacific block, $\lambda_W = 180°$, $\lambda_E = 140°$W, $\phi_S = 36°$N, and $\phi_N = 76°$N; for the Atlantic block, $\lambda_W = 10°$W, $\lambda_E = 30°$E, $\phi_S = 34°$N, and $\phi_N = 74°$N. The quantity $\overline{\psi_b}$ measures the central amplitude of the blocking anomaly. Since this simple function cannot completely fit the observed blocking pattern, we use a parameter α to control the gradient of ψ_b. We obtain very similar results when $1 \leq \alpha \leq 2$, which implies that the prescribed value of α in this range does not appreciably affect the calculated sensitivities. We use $\alpha = 1.5$. Figure 3 shows ψ_b, for the Pacific and Atlantic blocks when the amplitude $\overline{\psi_b}$ is 4.5×10^7 m^2 s^{-1} and 3.0×10^7 m^2 s^{-1}, respectively. Based on the composite analyses of Nakamura et al. (1997) and Michelangeli and Vautard (1998), we take the model time integration "window," that is, $t - t_0$ in (2.7), as 4 days. The time t_0 is the time when we perturb $x(t_0)$ by $\delta x(t_0)$. It is arbitrary since we are using a time-invariant climatological flow.

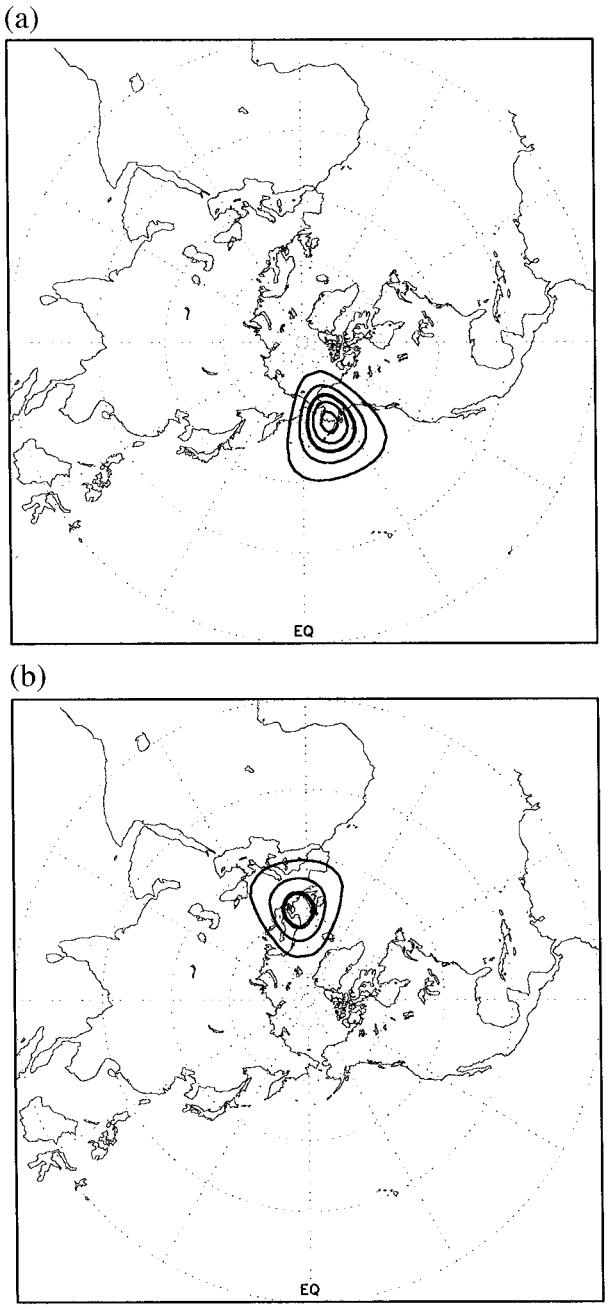

FIG. 3. The empirically selected (see text) anomalous streamfunction of blocking patterns used in the definition of the blocking indices for the Pacific (a) and Atlantic (b) block. The contour interval is 1.0 $\times 10^7$ m^2 s^{-1}, and the heavy line is for 2.1×10^7 m^2 s^{-1}.

a. Pacific block

We employ the just defined Pacific blocking index and study the dynamics of block onset over the Pacific. Figure 4 shows the wind vector field associated with the sensitivity perturbation, which is scaled with its maximum wind amplitude of 10 m s^{-1}, a value comparable to the wind intensity in atmospheric disturbances. An interesting flow signature is the presence of of the perturbation westerly winds over the Pacific between 25° and 35°N, which cause an advection of the high PV from the north of the jet core toward the central Pacific. We also observe a tropical flow signature consisting of three narrow and elongated eddies found between 0°–30°N and 90°E–140°W.

The vorticity field corresponding to the sensitivity wind vectors is presented in Fig. 5. The vorticity fields are primarily characterized by a wave train structure. Over the region near the Philippines the vorticity exhibits a positive center in the upper level, but a negative value in the lower level, that is, they are out of phase. The structures associated with the sensitivity perturbation are baroclinic over the Tropics and the subtropics. In middle and high latitudes, the structures are equivalent barotropic. The most important eddy feature has its major axes directed from northwest to southeast. From the Rossby wave ray theory, perturbation energy propagates along the direction parallel to the wavenumber vector, which is nearly perpendicular to the elongated axis in highly anisotropic eddies (Zeng 1983; Hoskins et al. 1983). The vorticity structure of the sen-

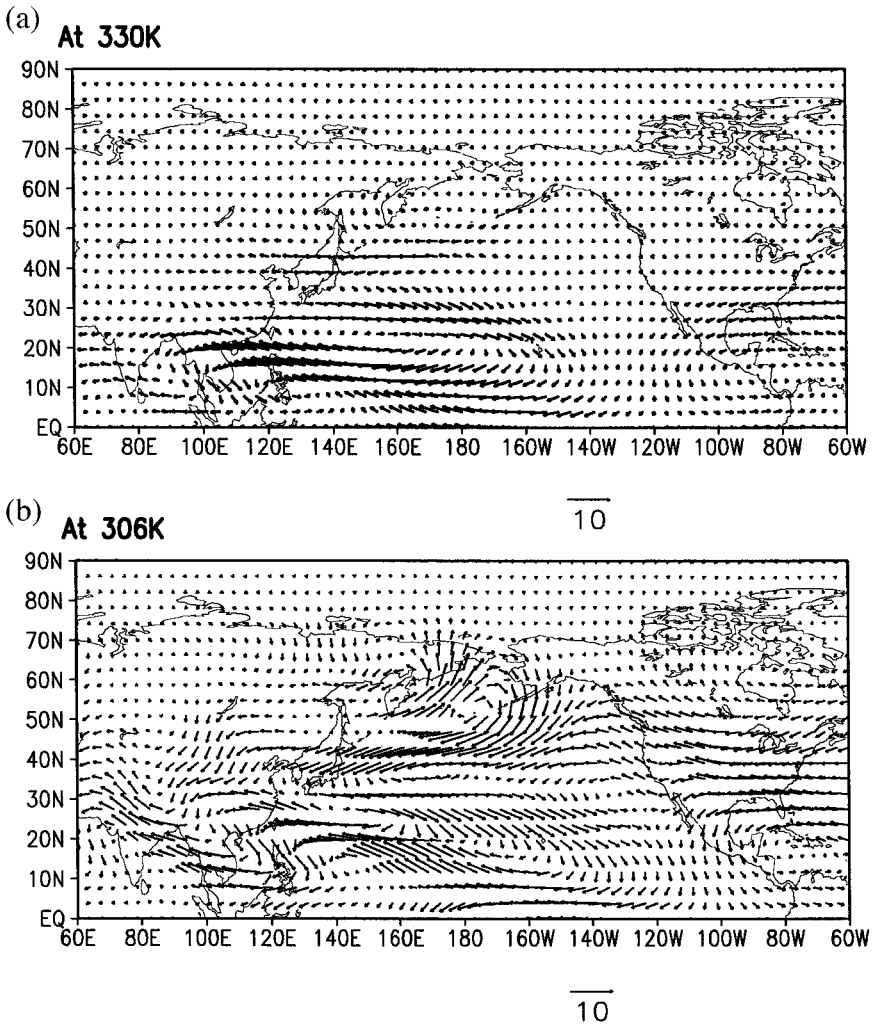

FIG. 4. Sensitivity wind vectors at the initial time for the Pacific blocking, no larger than 10 m s^{-1}. The background flow is the Jan climatological mean from 1984 to 1993. The time window $t - t_0$ is 4 days.

sitivity perturbations seems to ensure that eddy perturbation energy propagates toward the northeast.

We integrate the linearized model for 4 days using the sensitivity perturbation (Fig. 4) as the initial condition. Figure 6 shows the total streamfunction field at day 4 on the two θ surfaces. A typical block forms with its center midway on the string of the Aleutian Islands. Figure 7 displays the day-by-day evolution of the perturbation on the upper (Fig. 7a) and lower (Fig. 7b) θ surfaces. The columns, counted from the left, represent the perturbation streamfunction field, the perturbation PV field, and the total PV field. The rows, counted from the top down, show flow fields for days 1, 2, 3, and 4.

On day 1, the perturbation streamfunction exhibits a Rossby wave packet made up of three dominant eddies: The first and most eastward eddy is cyclonic with the second-largest amplitude, the second is anticyclonic with the largest amplitude, while the last eddy is cyclonic and has the weakest amplitude. These eddies have a pronounced, but different, horizontal tilt, which is greatest for the leading cyclonic eddy. They tilt against the horizontal shear of the Pacific jet and extract kinetic energy from the jet (Simmons et al. 1983; Zeng 1983). They also possess vertical tilts since the upper-layer perturbation centers lag the lower-layer ones by about one-quarter wavelength in the Tropics and subtropics. Such a vertical structure is conducive to baroclinic energy conversion. The evolution of the perturbations also shows that horizontal shear rotates the horizontal phase lines of these eddies and reduces their horizontal total wavenumber resulting in a growth of their horizontal scales. This is a situation in which baroclinic and barotropic processes both contribute to the nonmodal growth of the perturbation (Barcilon and Bishop 1998).

From the total PV field shown in the last column there is a diffluence in the PV contours associated with the

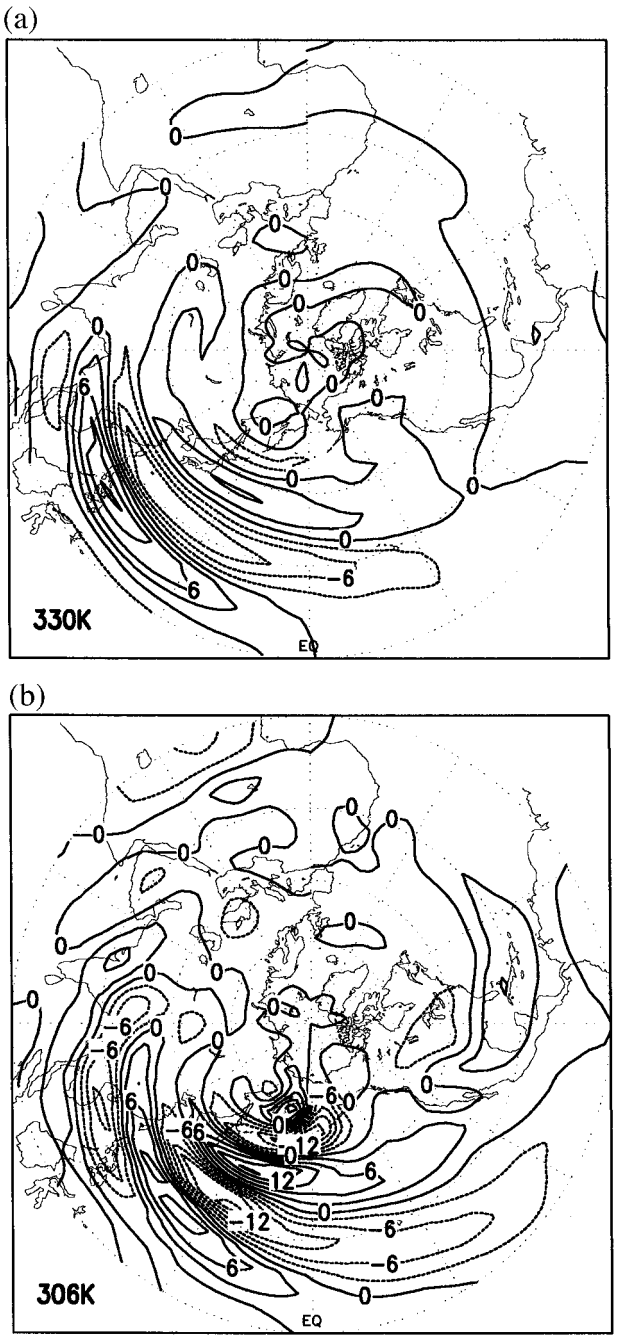

FIG. 5. Relative vorticity corresponding to the wind vectors in Fig 4. The contour values are scaled by 10^{-6} s^{-1}.

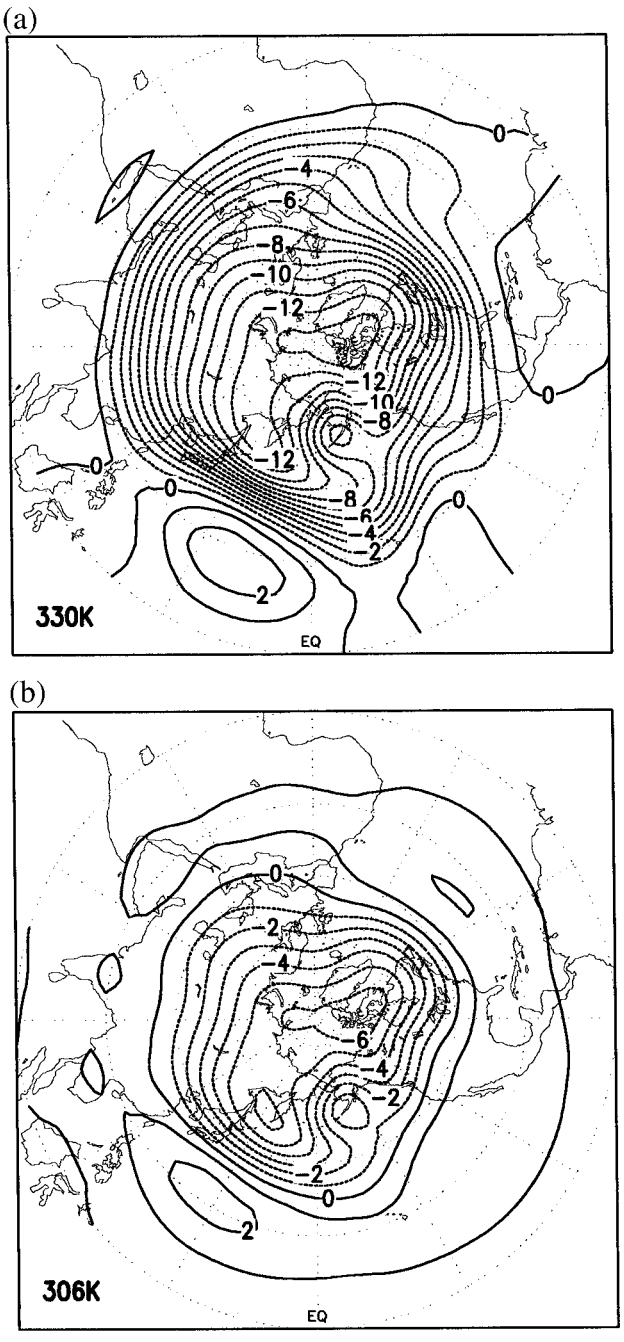

FIG. 6. The superposition of the streamfunction of the climatological mean and perturbation streamfunction obtained as the solution of the linear model at day 4. The contour values are scaled by 10^7 m^2 s^{-1}.

climatological ridge (or low PV trough), with the bunching of these contours in southward and northward branches. The bunching of these contours creates sharper horizontal PV gradient zones, which play the role of waveguides (Hoskins et al. 1985). As seen in Fig. 1, the Rossby wave packet lies mostly on the southern PV waveguide. Also seen in the perturbation streamfunction is a weak anticyclonic eddy found on the northern PV waveguide. Through their Lagrangian displacements to the southeast, both the leading cyclonic and anticyclonic eddies advect high PV from the jet's background PV reservoir to the midlatitude central Pacific, that is, the region south of where the block forms. In the second column, the perturbation PV shows the signature of the

wave packet and the formation of a tear-shaped high PV perturbation region on the northern PV waveguide.

On day 2, there is no phase propagation of the Rossby wave packet: it is stationary as noted in observations (Nakamura 1994; Nakamura et al. 1997). We conjecture that as a consequence of the Rossby wave energy emanating from the eddies in the wave packet, a significant positive perturbation streamfunction center has been established in the blocking area. The leading cyclonic eddy intensifies its PV by barotropic–baroclinic growth and increases its scale by clockwise rotation of its tilt as theoretically indicated by Zeng (1983), Hoskins et al. (1985), and Barcilon and Bishop (1998). Through the scale effect that eddy induces stronger winds that, on its northeast side, advect low PV to the northwest from the tropical low PV reservoir. The tilts of these eddies seems to play an important role in placing these advections of high and low PVs in the required location. The Rossby wave energy emanating from each eddy is propagating in a direction nearly perpendicular to its major axis and the energy propagation speed is proportional to the basic flow speed (e.g., Zeng 1983; Hoskins et al. 1983). Because of the particular eddy anisotropy and the weak basic flow in the climatological ridge (Fig. 1), we conjecture that energy is focused in the region of the weak anticyclone found on the northern PV waveguide and contributes to the buildup of the blocking ridge. We note the importance of PV advection in mechanisms associated with block onset, a fact already pointed out by Nakamura and Wallace (1993).

On day 3, the high–low couplet in the streamfunction anomaly continues to amplify and by day 4 it becomes the blocking dipole. The anticyclone attains a maximum streamfunction anomaly of 4.0×10^7 m^2 s^{-1}, which is equivalent to about 400 m in geopotential height. This value is close to that of the strongest block composite studied by Nakamura et al. (1997).

From the perturbation streamfunction evolution at the upper level, the strongest center in the perturbation wave train has a maximum of 1.0×10^7 m^2 s^{-1} at day 1. At day 4, the positive center associated with the block attains a maximum of 4.0×10^7 m^2 s^{-1}, implying a growth rate that more than doubles the amplitude of the perturbation in two days.

This time evolution seems in accord with atmospheric observations (e.g., Nakamura and Wallace 1993; Nakamura 1994; Colucci and Alberta 1996; Nakamura et al. 1997). We have displayed our results in terms of streamfunction. Through its inverse dependence on the Coriolis parameter, the streamfunction representation in the present study gives more importance to weak flow signatures in the Tropics and subtropics.

b. Atlantic blocks

In this study we do not distinguish between Atlantic and European blocks. We use the Atlantic blocking index and the observed climatology to construct the sensitivity perturbation. Figure 8 shows the winds associated with that perturbation scaled having a maximum of 10 m s^{-1}. The signature of sensitivity perturbation, when expressed in terms of vorticity, is shown in Fig. 9. It displays a less intense wave packet on the lower θ-surface than the one in the upper θ-surface. The eddies are anisotropic with different horizontal tilts.

We use this sensitivity perturbation as our initial condition and compute the evolution of the perturbation. After 4 days an omega block develops in the Bay of Biscay, north of Spain (Fig. 10). To show the evolution to block onset, we construct Figs. 11a,b in a similar fashion to Figs. 7a,b. In Fig. 11 on day 1, the perturbation streamfunction in the upper θ-level shows a wave packet consisting of three eddies in cyclonic–anticyclonic–cyclonic formation aligned in a southwest–northeast direction; also associated with the leading cyclonic eddy is a weak anticyclonic eddy north-northwest of that low. This perturbation streamfunction signature is clearly seen in the perturbation vorticity pattern in that figure. The total PV field displays a region of diffluence found ahead of the wave packet.

On day 2, the weak anticyclone is now the leading eddy in the Rossby wave packet consisting of four eddies, cyclonic–anticyclonic–cyclonic–anticyclonic. The horizontal tilts associated with these eddies fan out as four open fingers. The strong middle anticyclone and the cyclone to its east advect positive PV drawing from the jet PV reservoir. The leading anticyclonic–cyclonic pair advects negative PV from the Tropics. On day 3, the last anticyclonic–cyclonic pair of eddies on the Rossby wave packet weaken and probably lose their energy to the leading anticyclonic–cyclonic couplet, which grow. On day 4, the largest eddy is the blocking ridge.

c. Differences between the Pacific and Atlantic blocking

There exist some interesting differences between Pacific and Atlantic block onsets. The sensitivity perturbation uses the most effective way to create the low and high PV centers associated with blocks taking into account the flow and PV features of the jet. Thus different flow and PV features associated with the two jets may lead to differences between Pacific and Atlantic block onset.

The sensitivity perturbation for the Pacific block evolves into a dipole structure, while that associated with the Atlantic block maintains and amplifies the wave train signature across the Atlantic, a feature noted in the observations (Nakamura 1994; Nakamura et al. 1997; Michelangeli and Vautard 1998) and in numerical experiments (e.g., Michelangeli and Vautard 1998). Also, in our linear integrations, the time evolution of perturbation centers and their strengths are consistent with observations, especially those of Nakamura et al. (1997). The formation of the dipole structure in the

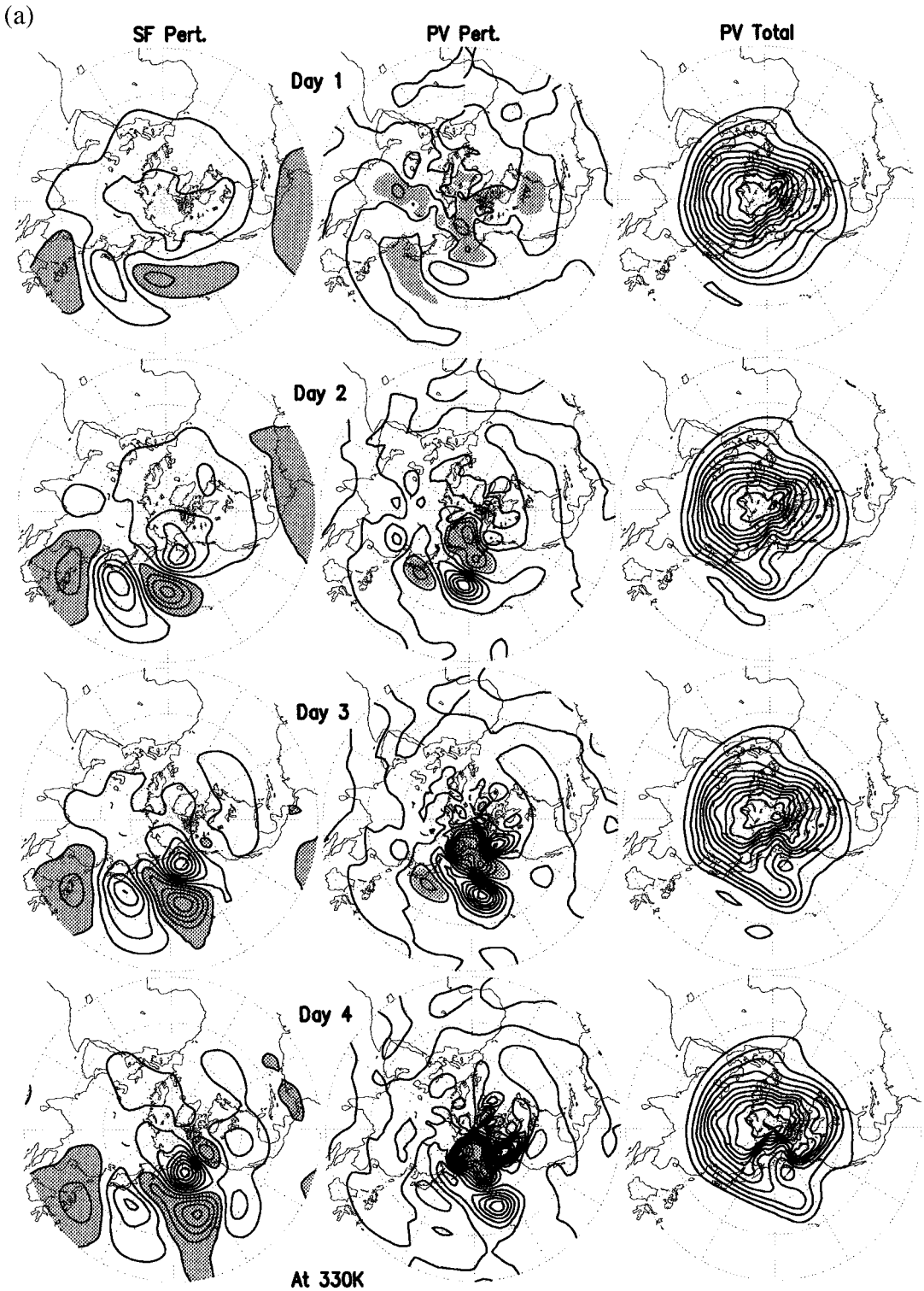

FIG. 7. Time evolution of three fields: the perturbation streamfunction in column one (left), the perturbation IPV in column two (center), and the superposition IPV in column three (right). Each row corresponds to a given day starting with the first day. At 330 K (a), the contour interval is 0.5×10^7 m^2 s^{-1} for the perturbation streamfunction and negative values are shaded; the contour interval is 0.4 PV unit for the perturbation IPV, and values smaller than -0.02 PV unit

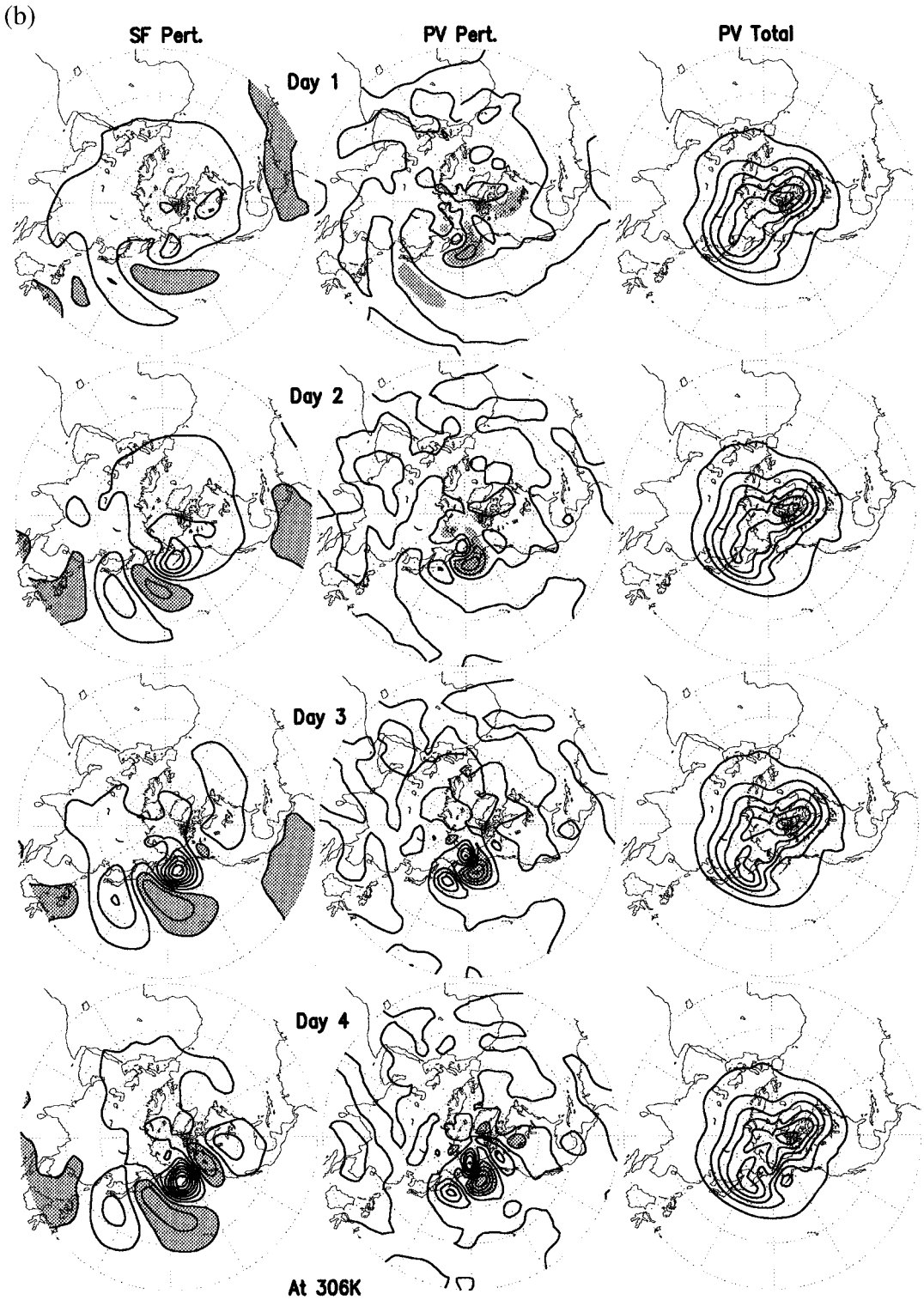

FIG. 7. (*Continued*) are shaded; the contour interval is 1.0 PV unit for the superposition IPV. At 306 K (b), the contour interval is the same as that at 330 K for the perturbation streamfunction; the contour interval is 0.2 PV unit for the perturbation IPV, and values smaller than −0.02 PV unit are shaded; the contour interval is 0.5 PV unit for the superposition IPV.

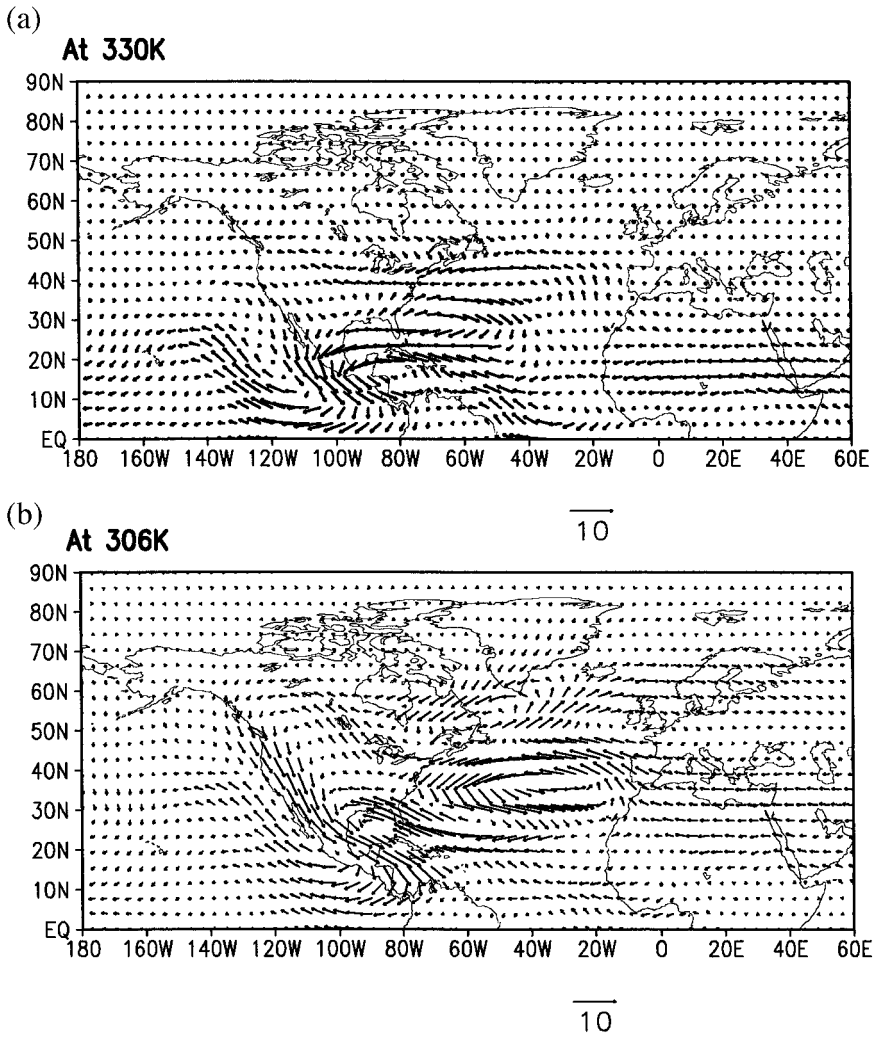

FIG. 8. Same as in Fig. 4 but for the Atlantic block.

Pacific block onset does not seem to have attracted much attention. In fact, we can discern this dipole structure in the composites studied by Nakamura et al. (1997). Their negative center south of the block is not as strong as the one associated with the sensitivity perturbation because Nakamura et al. display their data using geopotential height fields, which place more importance on high-latitude systems. Thus, relative weak centers at lower latitudes are less evident.

Differences between the PV dynamics associated with the onset of Pacific and Atlantic blocks are also noteworthy. Over the Pacific the wave train from the very start exhibits a clear baroclinic structure, implying presence of both baroclinic and barotropic instabilities (Barcilon and Bishop 1998). The Pacific eddies are larger than the Atlantic ones; there is an out of phase difference between PV and streamfunction consistent with the ideas of Lagrangian PV advection. In the Atlantic the wave train has a much more pronounced barotropic structure and baroclinic phase tilts are much smaller implying the preponderance of barotropic instability. The leading anticyclonic–cyclonic pair of eddies, which make up the Rossby wave train, become the omega block. Correspondingly, the growth rates of sensitivity perturbations of the Atlantic block are smaller than those of the Pacific block.

4. Sensitivity forcing

Recent numerical simulations and observation diagnostics have suggested that block onset may be excited by external forcing, such as vorticity sources related to anomalous SSTs (e.g., Ferranti et al. 1994; Hoskins and Sardeshmukh 1987; Sardeshmukh and Hoskins 1988). We introduce the concept of sensitivity forcing and investigate the physical processes associated with excitation of blocking by means of an external forcing.

When the initial value of the perturbation is zero, we may write the solution to the forced problem found in (2.2) as

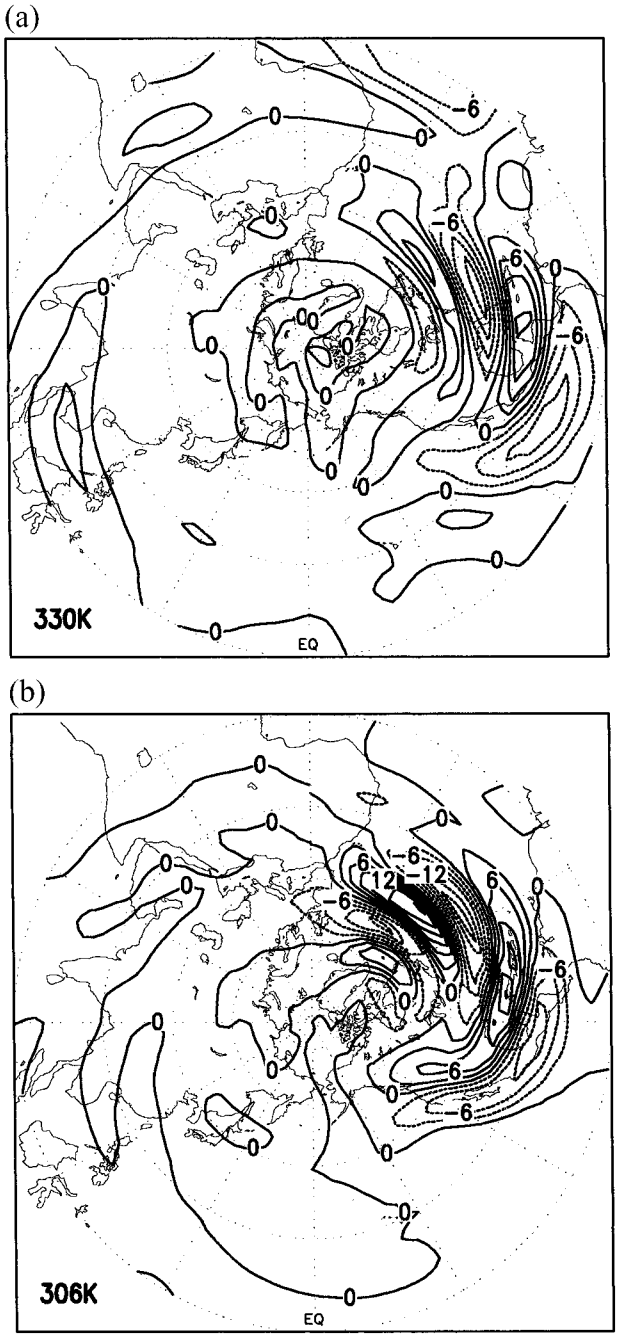

FIG. 9. Same as in Fig. 5 but for the Atlantic block.

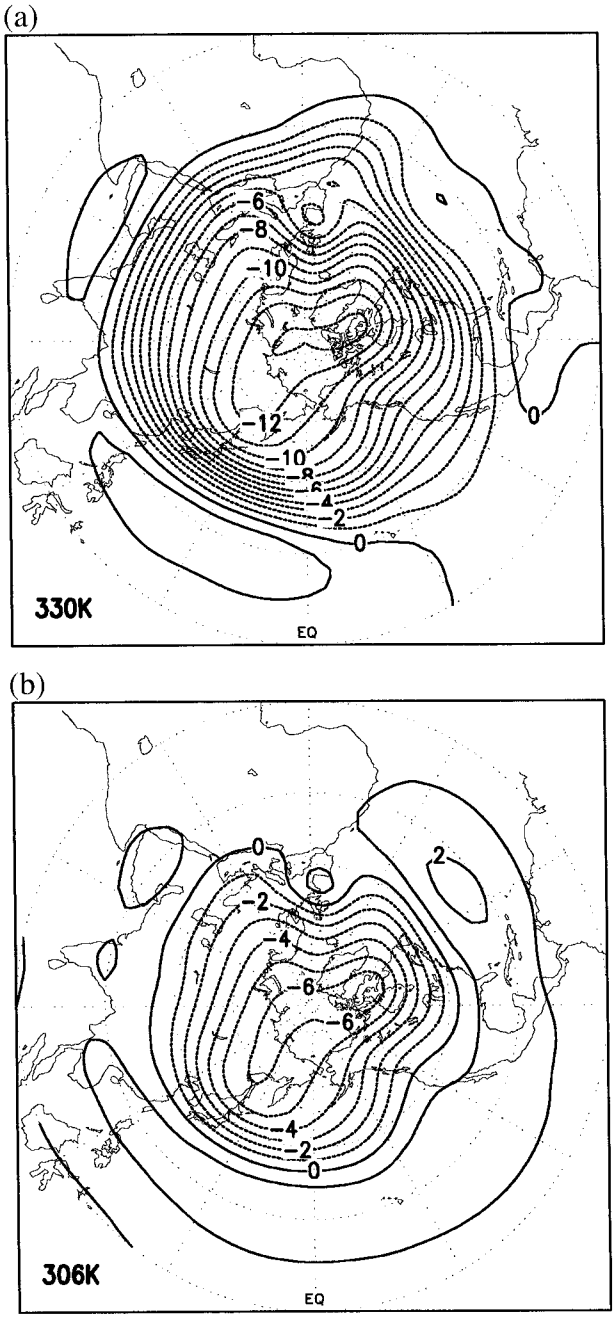

FIG. 10. Same as in Fig. 6 but for the Atlantic block.

$$\delta x(t) = \int_{t_0}^{t} \mathbf{A}(t, t - \tau)\, d\tau \cdot \delta F. \tag{4.1}$$

Here, δF is the perturbation forcing and $\mathbf{A}(t, t - \tau)$ the resolvent as defined in section 2c. Assume that δF is stationary. This may not be a bad approximation if the timescale of the external forcing is much greater than a few days, characteristic of the timescale for block onset. Then, substituting (4.1) into (2.6), we obtain

$$\delta R = \left\langle \int_{t_0}^{t} \mathbf{A}(t, t - \tau)\, d\tau \cdot \delta F, x_b \right\rangle \Big/ \langle x_b, x_b \rangle$$

$$= \left\langle \delta F, \int_{t_0}^{t} \mathbf{A}^{\mathrm{T}}(t, t - \tau)\, d\tau \cdot x_b \right\rangle \Big/ \langle x_b, x_b \rangle. \tag{4.2}$$

Comparing (4.2) with (2.5), we may write the gradient of the response function with respect to the forcing F as

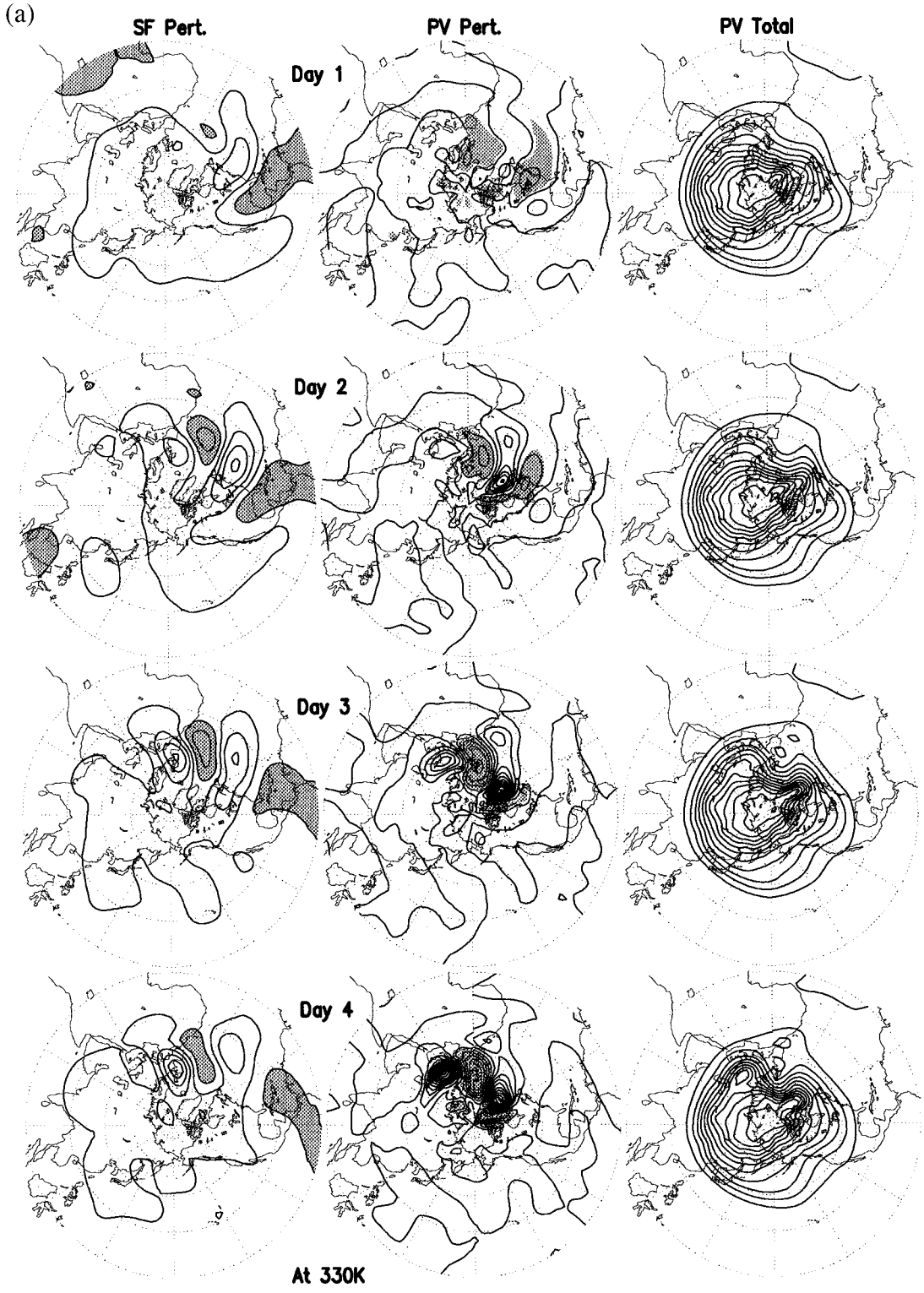

FIG. 11. Same as in Fig. 7 but for the Atlantic block.

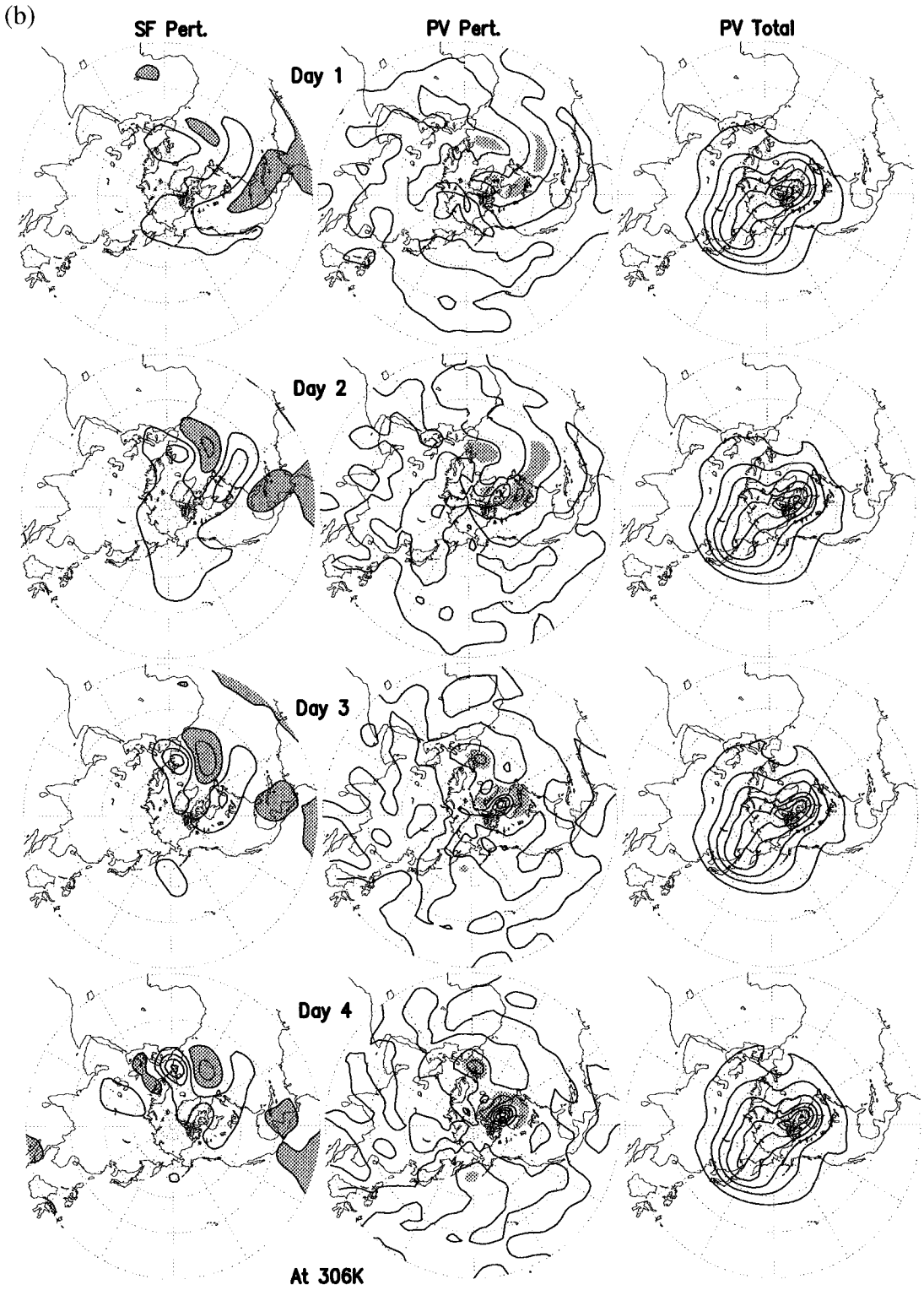

FIG. 11. (*Continued*)

$$\nabla_F R = \int_{t_0}^{t} \mathbf{A}^{\mathrm{T}}(t, t - \tau)\, d\tau \cdot x_b / \langle x_b, x_b \rangle. \quad (4.3)$$

In the time discretized form $t_0 < t_1 < \cdots < t_J$, (4.3) becomes

$$\nabla_F R = \sum_{j=1}^{J} \Delta t_j \mathbf{A}^{\mathrm{T}}(t, t - t_{j-1}) x_b / \langle x_b, x_b \rangle, \quad (4.4)$$

where $\Delta t_j = t_j - t_{(j-1)}$ is the model time integration step length and J the model total integration step number. To calculate $\nabla_F R$, define a vector $\mathbf{G}$ of the same dimension as $\nabla_F R$ and set it to zero initially; integrate the adjoint model backward in time from t_J to t_0 using x_b as the initial condition at t_J; when the adjoint model is integrated to the time t_j, multiply the integration value by Δt_j and add it to $\mathbf{G}$. Scale the final value of $\mathbf{G}$ by $\langle x_b, x_b \rangle$ to obtain $\nabla_F R$. Then, $\nabla_F R$ can be calculated by a single backward integration of the adjoint model.

In this isentropic model, the perturbation forcing vector, δF, consists of vorticity-, divergence-, and diabatic-heating forcing (see the appendix). As previously discussed for sensitivity initial perturbations, we may analyze forcing functions related to F, say $F = \mathbf{C}g$; then the gradient of the response R with respect to the new forcing function g is given by

$$\nabla_g R = \mathbf{C}^{\mathrm{T}} \nabla_F R. \quad (4.5)$$

In fact, similar to our findings pertaining to initial perturbations discussed in section 3, our calculations show that only the sensitivity forcing associated with the wind components can excite typical blocking patterns. In other words, we write the vorticity source as $\mathbf{k} \cdot \nabla \times \mathrm{v_f}$, the divergence source as $\nabla \cdot \mathbf{v_f}$, and the diabatic heating source as H_f (see the appendix). Then $\mathrm{v_f}$ and H_f constitute the vector forcing function g.

We first perform the sensitivity forcing analysis for the Pacific block. Figure 12 illustrates the sensitivity vorticity forcing, $\mathbf{k} \cdot \nabla \times \mathbf{v_f}$. The vorticity forcing is very similar to the initial structures found in the sensitivity perturbation based on vertical vorticity (see Fig. 5). Figure 13 displays the streamfunction of the linear response to the sensitivity vorticity forcing at day 4. We observe a typical Pacific block, similar to the one shown in Fig. 6.

The time evolution of block onset by the sensitivity vorticity forcing is very similar to that obtained by using the initial sensitivity wind components. In the initial value problem, perturbations grow due to the efficient extraction of barotropic and baroclinic energy from the background flow. In fact, the sensitivity vorticity forcing has a structure similar to an efficient forcing mode defined by the leading singular vector (see Li and Ji 1997).

An important feature of the sensitivity vorticity forcing is its emphasis on the tropical western Pacific, especially the area near the Philippines. Ferranti et al. (1994) performed numerical experiments showing that the SST anomaly near the Philippines has a major impact on Pacific blocking activity. Diagnostics and numerical experiments with simple barotropic models have indicated the crucial importance of vorticity gradients in the vicinity of the east Asian jet (e.g., Simmons 1982; Simmons et al. 1983; Sardeshmukh and Hoskins 1988). We can clarify this picture by using PV thinking. The sensitivity vorticity forcing localized near the Philip-

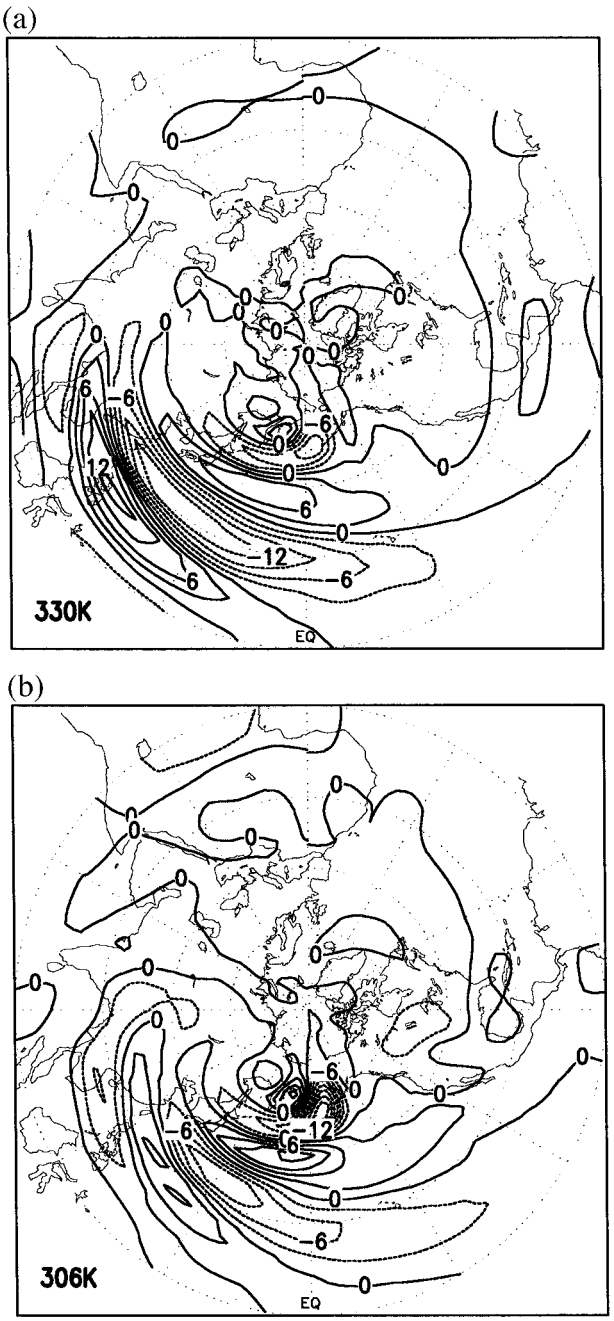

FIG. 12. Sensitivity forcing of vorticity for the Pacific blocking, which is scaled to attain a maximum of 1.5×10^{-10} s^{-2} near the Philippines. The contour interval is 3.0×10^{-11} s^{-2}. The background flow is the Jan climatological mean from 1984 to 1993. The time window $t - t_0$ is 4 days.

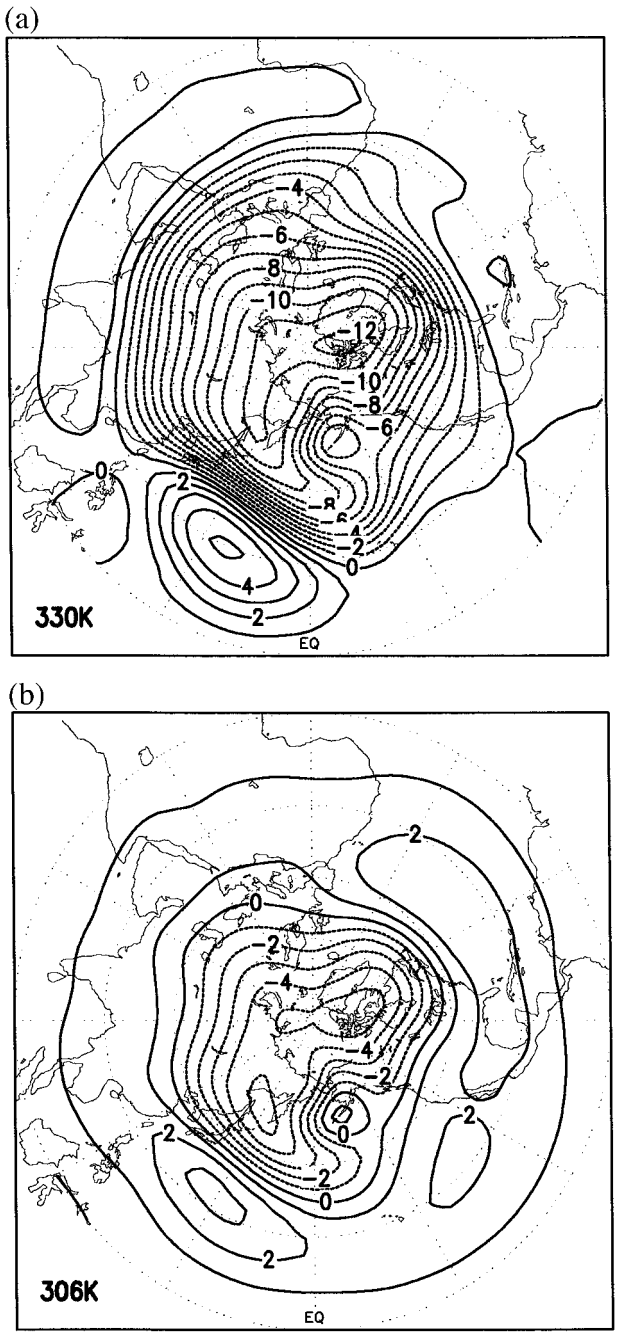

FIG. 13. The superposition streamfunction of the climatological mean and the response of the perturbation streamfunction in the linear model at day 4 for the Pacific blocking. The contour interval is 10^7 m^2 s^{-1}.

pines acts like a ''paddle'' and produces flow perturbations that cause efficient advection of the high PV, leading to the creation of the anomalous high PV center in the region immediately south of where the block forms.

We now examine the strength of the vorticity forcing shown in Fig. 12. The main centers near the Philippines have a strength of about 1.5×10^{-10} s^{-2}. In the Tropics, this vorticity source is equivalent to that produced by a divergence of 2.0×10^{-6} s^{-1}. From the estimates given by Hoskins and Karoly (1981), this value of divergence corresponds to an additional 5 mm of rain per day. Such a strength of anomalous vorticity sources appears to be readily attainable in the atmosphere. However, whether there exists vorticity forcing having a structure similar to sensitivity structures remains a concern. ''Exact'' sensitivity structures are not necessary; a vorticity forcing induced by the secondary circulation due to SSTs or due to other mechanisms may excite a block if its pattern has a sufficiently large projection onto the sensitivity structure.

Figure 14 presents the sensitivity vorticity forcing for the Atlantic blocking, and Fig. 15 its linear response at day 4. Discussions applicable to the Pacific blocking are also applicable to the Atlantic blocking. The main features of sensitivity vorticity forcing of the Atlantic blocking are related to the Atlantic jet. The sensitivity vorticity forcing is primarily localized on the south flank and in the exit area of the jet over the northeast Atlantic. The geographical location of this sensitivity area is consistent with that found by numerical experiments (Ferranti et al. 1994) and observational diagnoses (Hoskins and Sardeshmukh 1987).

Thus, external forcings may excite blocking through their induced vorticity source. This statement does not contradict the results of the numerical experiments of Ferranti et al. (1994) that show the significant effects of anomalous SSTs on blocking. An anomalously warm ocean may induce enhanced convective heating in the atmosphere. This heating will be balanced by enhanced upward motion, which will, in turn, induce divergence and forcing of anticyclonic vorticity at upper levels (e.g., Sardeshmukh and Hoskins 1988). Our results are a consequence of the fact that the vorticity source described above can be thought as the ''paddle'' or forcing mechanism, which generates the Rossby waves.

5. Discussion

In this study we view block onset as a consequence of the evolution of localized perturbations in a background flow. We attempted to answer the question, what are the characteristics of synoptic perturbations that may directly evolve into blocking patterns, and what are the dynamics associated with the evolution of such synoptic perturbations leading to block onset? For these disturbances, we answered the second part of that question by proposing a PV framework, which describes the various mechanism leading to block onset. As such, we believe this framework to be a valuable contribution to this area of research. We hope, in the near future, to undertake quantitative research that may corroborate our views. As mentioned previously, because of the suspected plurality of mechanisms of block onset, this pro-

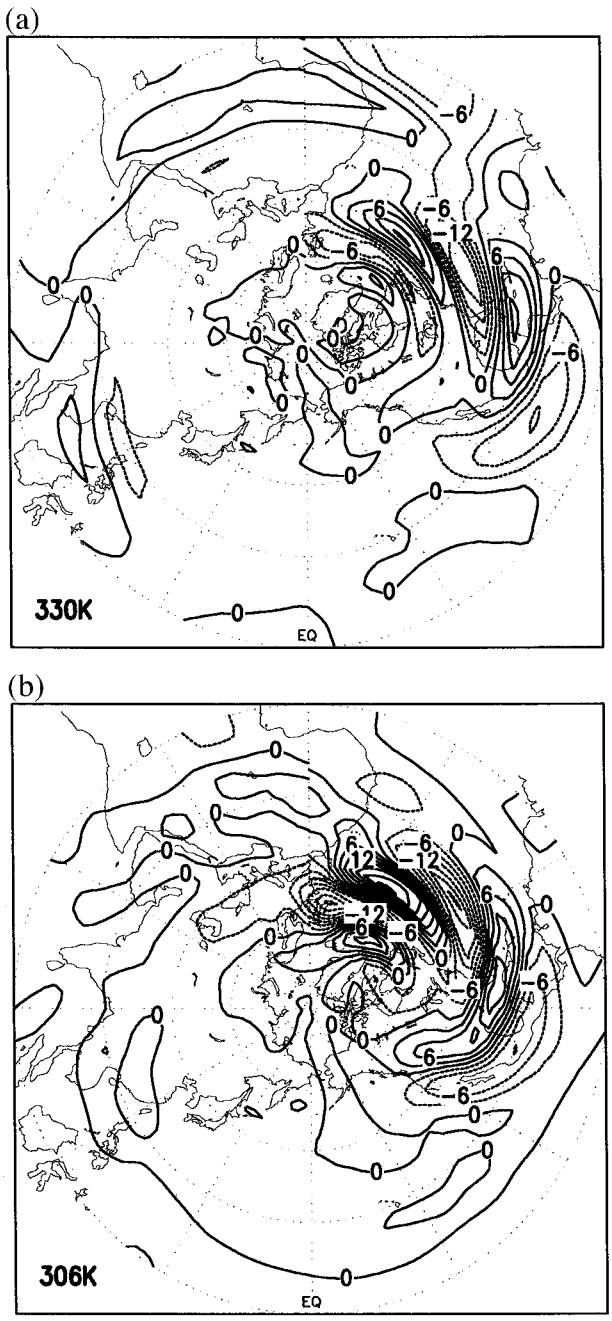

FIG. 14. Sensitivity forcing of vorticity for the Atlantic blocking, which is scaled to be the maximum of 1.5×10^{-10} s^{-2} near the Caribbean. Others are the same as in Fig. 12.

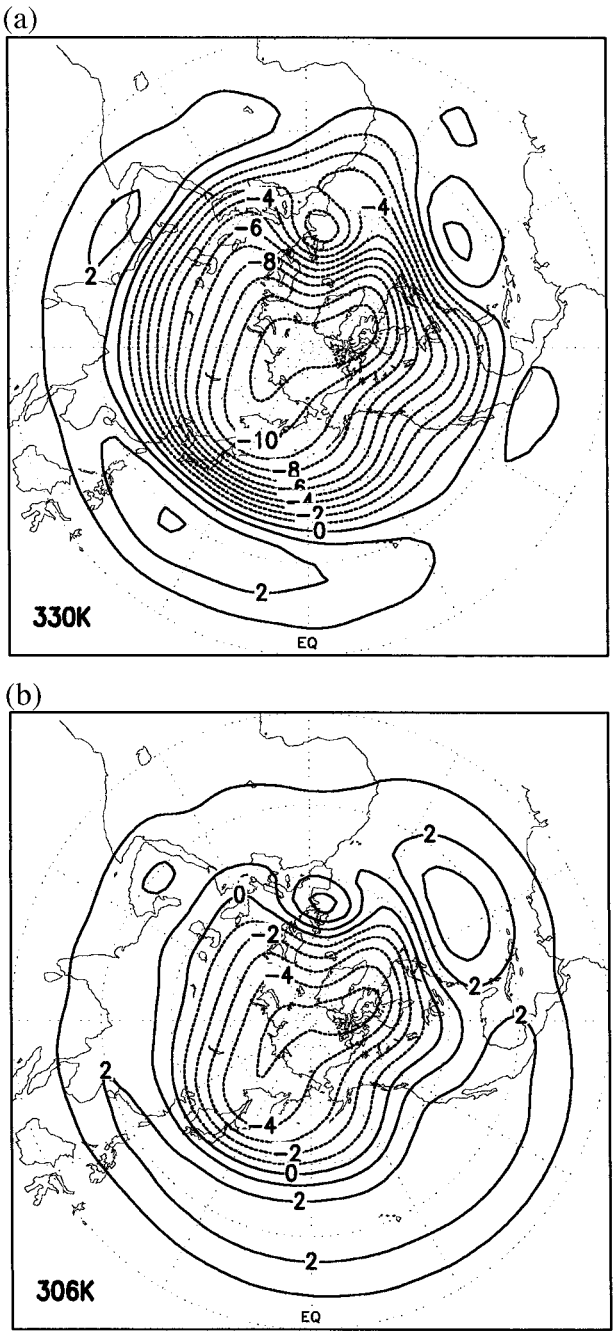

FIG. 15. Same as in Fig. 13 but for the Atlantic blocking.

posed mechanism may be one among many that leads to block onset.

We employed sensitivity analysis to compute the initial perturbation, designated as the sensitivity perturbation. After 4 days, this initial perturbation produced the maximum change in a given blocking index. We argued that the synoptic perturbation that can directly evolve into a blocking pattern should have a large projection on these sensitivity perturbations. We further generalized sensitivity analysis to forced problems. With similar methods, we computed the sensitivity forcing perturbation that produces the maximum change in the blocking index after 4 days. The assumed quasi-stationary forcings may be a result of atmospheric secondary circulations driven by anomalous heating, vorticity, or divergence sources or other mechanisms not detailed in this work.

We focused on one mechanism of block onset, which is embedded in the climatological January flow of the Northern Hemisphere. We argued that composites of observations of block onset (Nakamura 1994; Nakamura et al. 1997; Michelangeli and Vautard 1998) produced conditions similar to those prevailing in the climatological flows and therefore we were justified in comparing the results of our experiments with these sets of observations. Yet the mechanism of block onset we discussed may not be the *only* one. Block onset due to planetary Rossby wave breaking (Pondeca et al. 1998a,b) and other mechanisms may also excite block onset.

In our sensitivity analyses, the model climatological flow was derived from observed January data for 10 yr, which consist of mean monthly reanalyses of NASA DAO from 1984 to 1993. We limited our investigations to Pacific and Atlantic block onsets. Results showed that sensitivity perturbations expressed in terms of winds no greater than 10 m s^{-1} can excite blocking. We expressed the sensitivity perturbation forcing in terms of the vertical vorticity source. In this model, the vorticity source with an intensity less than 1.5×10^{-10} s^{-2} was sufficient to produce block onset. This numerical value corresponds to a divergence of the order of 2.0×10^{-6} s^{-1}, a very realizable magnitude for divergence under usual tropical conditions. We suggested that sensitivity perturbations or forcing of modest strength can excite block onset even with climatological flows as the background model state.

The flow structure of the sensitivity perturbation and forcing perturbation may provide block precursors. For the Pacific and Atlantic blocking indices, the sensitivity perturbation and sensitivity forcing had well-organized signatures when expressed in terms of vertical vorticity. These signatures consisted of Rossby wave train structures containing elongated eddies mainly localized on the southern flank of the jets. For Pacific blocks, the sensitivity perturbation and sensitivity forcing had their largest amplitudes in the area of the Philippines, especially in the upper model atmosphere. For the Atlantic blocks, the sensitivity perturbation and sensitivity forcing had their largest amplitudes over the Caribbean area. These two regions have common characteristics: they are located south of the jets and near the jets' exit areas. They are also in the Tropics. The Rossby wave trains are quasi-stationary and constitute an essential organizing feature rooted in PV dynamics, which induced the correct Lagrangian displacements. We argued that perturbations excited by the sensitivity forcing undergo a rapid growth by extracting energy from the background flow through both barotropic and baroclinic processes. The importance of the Philippines and Caribbean regions for the block onset have been noted in numerical experiments (e.g., Ferranti et al. 1994) and diagnostic studies (Hoskins and Sardeshmukh 1987; Sardeshmukh and Hoskins 1988).

We have emphasized the role of the sensitivity perturbation and of sensitivity forcing in the Tropics. Tropical sensitivity perturbations may result from a given phase of the intraseasonal disturbances, possibly associated with the convection anomaly dipole of the Madden–Julian Oscillation. Intriguing candidates are also high-frequency (a few days) disturbances, which propagate down into the Tropics from midlatitudes. Sensitivity forcing may primarily be associated with atmospheric secondary circulations driven by anomalous heating, vorticity, or divergence sources. In the near future, we hope to verify such linkage by using observational data analysis.

The perturbation produced by sensitivity forcing strongly interacts with the background flow and effectively extract energy from that flow. Energetics calculations performed by Li and Ji (1997) found that the energy of the perturbations produced by the sensitivity forcing are mainly due to the local extraction of energy from the jets. When the perturbation propagates away from the wave source, the dynamics of the perturbation evolution is primarily determined by its *local* interaction with the background flow. Finally, according to our dynamical scenario, the background flow controls the space and time characteristics of block onset. This also implies that the space and time characteristics of block onset may be nearly independent of the mechanisms, which may have initially caused these perturbations.

For the Pacific block the mechanistic picture we envisaged is as follows: the sensitivity perturbation near the Philippines acts as a ''paddle'' and induces a PV standing wave on the strong background PV gradients associated with the jet. These regions of strong PV gradients act as PV wave guides. The Rossby wave train consists of three eddies, the leading one being cyclonic. These eddies possess vertical tilts associated with baroclinic instability as well as strong, but different, horizontal tilts. These eddies induce Lagrangian displacements, which advect both high and low PV from the high PV reservoir associated with the jet and the low PV reservoir associated with the Tropics. Their horizontal phase tilt is such that the leading cyclonic eddy grows due to this advection of high PV. It also grows in scale. The scale effect associated with PV thinking (Hoskins et al. 1985) contributes to growth through more intense Lagrangian motions induced by these larger-scale eddies. Barotropic and baroclinic mechanisms cooperate during this growth (Barcilon and Bishop 1998). The leading cyclonic eddy produces an enhanced advection of low PV and is responsible for the buildup of the blocking ridge. We also conjectured that there exists a focusing of eddy energy in the very region where the blocking ridge develops. In our view, the key step in this chain of events leading to block onset is the growth of the leading cyclonic eddy by means of high PV Lagrangian advection.

For the Atlantic block we envisaged a similar mechanistic picture. The sensitivity perturbation has a vorticity wave train with its largest amplitude in the Ca-

ribbean region. There are two important differences between the evolution of Pacific and Atlantic flows leading to block onset. First, for the Pacific block onset the sensitivity perturbation evolves into a blocking dipole while for the Atlantic the sensitivity perturbation retains its wave train structure. Second, the eddies over the Pacific possess larger scales, are more intense, and have much more of an initial baroclinic structure than eddies found over the Atlantic. These two differences appear to be a consequence of the stronger jet and PV gradients in the western Pacific compared to those found over the western Atlantic.

How model dependent are our results? Because in our calculations the background flow is derived from the observed climatology, the model is merely used to calculate the linear evolution of perturbations away from the climatological flow. Therefore, our results should not be too sensitive to the model used. But, since the model resolution in the vertical is very low and all calculations are carried out in the linearized context, we must refrain from sweeping claims and regard these results as qualitative rather than quantitative. We expect to employ a more realistic general circulation model to further test the validity of these qualitative results and to perform detailed quantitative analysis in future studies.

Forecast of blocking onset is still one of the unsolved areas of research that strongly impacts medium- and extended-range forecasts. If the proposed mechanism of block onset is the one more likely to occur, observations near the Philippines and the Caribbean should be crucial for improved forecasting of the event. Yet, at the present time, they suffer from substantial errors, which may constitute one of the major obstacles in the forecast of blocking. The proposed mechanism of block onset also suggests that numerical weather prediction models ought to be skilled in tropical predictions for the improved forecast of blocking.

Acknowledgments. A. Barcilon gratefully acknowledges partial support from AFOSR Grant F49620-96-1-0172. Z. Li and I. M. Navon acknowledge the support from the NSF Grant ATM-9413050 managed by Dr. Pamela Stephens, whom we would like to thank for her support, and from the Supercomputer Computations Research Institute, which is partially funded by the Department of Energy through Contract DE-FG05-85ER250000. This is contribution number 401 of the Geophysical Fluid Dynamics Institute.

APPENDIX

Description of the Two-Layer Isentropic Model

Details of this model can be found in Zou et al. (1993). The model equations may be written in a vertically discretized form as

$$\frac{\partial \zeta_k}{\partial t} + \nabla \cdot [(A_k, B_k)] = \zeta_{\text{fk}}, \tag{A.1}$$

$$\frac{\partial D_k}{\partial t} + \nabla \cdot [(-B_k, A_k)] + \nabla^2 \left[g z_s + \frac{1}{2}(u_k^2 + v_k^2) \right] + \nabla^2 M_k' = D_{\text{fk}}, \tag{A.2}$$

$$\frac{\partial \Delta \pi_k'}{\partial t} + \nabla \cdot [(u_k \Delta \pi_k', v_k \Delta \pi_k')] + \Delta \overline{\pi}_k D_k = (-1)^k \frac{\theta_{3/2}}{C_p} \frac{(C_p + \pi_{5/2})}{\Delta \theta} H_{\text{fk}}, \tag{A.3}$$

$$\zeta_{\text{fk}} = \mathbf{k} \cdot \nabla \times \mathbf{v}_{\text{fk}}, \qquad D_{\text{fk}} = \nabla \cdot \mathbf{v}_{\text{fk}}, \qquad k = 1, 2, \tag{A.4}$$

where

$$A_k = u_k(\zeta_k + f) + \frac{\dot{\theta}_{3/2}(\Delta \pi_1 + \Delta \pi_2)}{2 \Delta \theta \Delta \pi_k}(v_2 - v_1) - \left(\alpha \nabla^{\nu} - \frac{\delta_{k1}}{\tau_{\text{drag}}} \right) v_k, \tag{A.5}$$

$$B_k = v_k(\zeta_k + f) - \frac{\dot{\theta}_{3/2}(\Delta \pi_1 + \Delta \pi_2)}{2 \Delta \theta \Delta \pi_k}(u_2 - u_1) + \left(\alpha \nabla^{\nu} - \frac{\delta_{k1}}{\tau_{\text{drag}}} \right) v_k, \tag{A.6}$$

$$\Delta \pi_k = \pi_{k-1/2} - \pi_{k+1/2}, \qquad \Delta \theta = \theta_2 - \theta_1, \tag{A.7}$$

$$\Delta \pi_k' = \Delta \pi_k - \Delta \overline{\pi}_k, \qquad \pi_{\text{mid}} = \frac{1}{2}(C_p + \pi_{5/2}), \tag{A.8}$$

$$\Delta \overline{\pi}_1 = C_p - \pi_{\text{mid}}, \qquad \Delta \overline{\pi}_2 = \pi_{\text{mid}} - \pi_{5/2}. \tag{A.9}$$

Here the lower level and upper level are designated by 1 and 2, respectively, and are at the midlevel of the two layers; the surface, the layer interface, and the top level are numbered 1/2, 3/2, and 5/2, respectively. Here θ is the potential temperature, $\kappa = R/C_p$, $\pi = C_p(p/p_0)^{\kappa}$ is the Exner function, and $M = \pi\theta + gz$. The parameters used are as follows: $\theta_1 = 306$ K, $\theta_2 = 330$ K, $p_0 = 100$ hPa, $z_{\text{top}} = 11\,500$ m, $\pi_{5/2} = C_p - gz_{\text{top}}/\theta_1, \nu = 6$, and $\tau_{\text{drag}} = 5$ days. Other notations are standard (see Zou et al. 1993). We have introduced a vorticity source ζ_{fk}, a divergence source D_{fk}, and a diabatic heating H_{fk}. In the linearized equations they have their perturbed counterparts.

In the sensitivity forcing analysis, we calculate the gradients of the response functions with respect to $\mathbf{v}_{\text{fk}}$ and H_{fk}, rather than with respect to ζ_{fk} and D_{fk}. Then we analyze H_{fk} as well as ζ_{fk} and D_{fk} as calculated from (A.4).

REFERENCES

Anderson, J. L., 1993: The climatology of blocking in a numerical forecast model. *J. Climate,* **6,** 1041–1056.

Barcilon, A., and C. Bishop, 1998: Nonmodal development of baroclinic waves undergoing horizontal shear deformation. *J. Atmos. Sci.,* **55,** 3583–3597.
Bengtsson, L., 1981: Numerical prediction of atmospheric blocking—A case study. *Tellus,* **33,** 19–42.
Black, R. X., and R. M. Dole, 1993: The dynamics of large-scale cyclogenesis over the North Pacific Ocean. *J. Atmos. Sci.,* **50,** 421–442.
Borges, M. D., and D. L. Hartmann, 1992: Barotropic instability and optimal perturbations of observed nonzonal flow. *J. Atmos. Sci.,* **49,** 335–354.
Branstator, G., 1987: A striking example of the atmosphere's leading traveling pattern. *J. Atmos. Sci.,* **44,** 2310–2323.
Colucci, S. J., 1985: Explosive cyclogenesis and large-scale circulation changes: Implications for atmospheric blocking. *J. Atmos. Sci.,* **42,** 2701–2717.
——, 1987: Comparative diagnosis of blocking versus nonblocking planetary-scale circulation changes during the synoptic-scale cyclogenesis. *J. Atmos. Sci.,* **44,** 124–139.
——, and T. L. Alberta, 1996: Planetary-scale climatology of explosive cyclogenesis and blocking. *Mon. Wea. Rev.,* **124,** 2509–2520.
Crum, F. X., and D. E. Stevens, 1988: A case study of atmospheric blocking using isentropic analysis. *Mon. Wea. Rev.,* **116,** 223–241.
Dole, R. M., 1986: The life cycle of persistent anomalies and blocking over the North Pacific. *Advances in Geophysics,* Vol. 29, Academic Press, 31–69.
——, 1989: The life cycle of persistent anomalies. Part I: Evolution of 500 mb height fields. *Mon. Wea. Rev.,* **117,** 177–211.
Ferranti, L., F. Molteni, and T. N. Palmer, 1994: Impact of localized tropical and extratropical SST anomalies in ensembles of seasonal GCM integrations. *Quart. J. Roy. Meteor. Soc.,* **120,** 1613–1645.
Frederiksen, J. S., 1982: A unified three-dimensional instability theory of the onset of blocking and cyclogenesis. *J. Atmos. Sci.,* **39,** 970–982.
——, 1983: A unified three-dimensional theory of the onset of blocking and cyclogenesis. Part II: Teleconnection patterns. *J. Atmos. Sci.,* **40,** 2593–2609.
——, 1997: Adjoint sensitivity and finite-time normal mode disturbances during blocking. *J. Atmos. Sci.,* **54,** 1144–1165.
——, and R. C. Bell, 1990: North Atlantic blocking during January 1979. Linear theory. *Quart. J. Roy. Meteor. Soc.,* **116,** 1289–1313.
Hansen, A. R., and A. Sutera, 1993: A comparison between planetary-wave flow regimes and blocking. *Tellus,* **45A,** 281–288.
Higgins, R. W., and S. D. Schubert, 1994: Simulated life cycle of persistent anticyclonic anomalies over the North Pacific: Role of synoptic-scale eddies. *J. Atmos. Sci.,* **51,** 3238–3260.
Hoskins, B. J., and D. J. Karoly, 1981: The steady linear response of a spherical atmosphere to thermal and orographic forcing. *J. Atmos. Sci.,* **38,** 1179–1196.
——, and P. D. Sardeshmukh, 1987: A diagnostic study of the dynamics of the Northern Hemisphere winter of 1985–1986. *Quart. J. Roy. Meteor. Soc.,* **113,** 759–778.
——, and T. Ambrizzi, 1993: Rossby wave propagation on a realistic longitudinally varying flow. *J. Atmos. Sci.,* **50,** 1661–1676.
——, I. N. James, and G. H. White, 1983: The shape, propagation and mean-flow interaction of large-scale weather systems. *J. Atmos. Sci.,* **40,** 1595–1612.
——, M. E. McIntyre, and A. W. Robertson, 1985: On the use and significance of isentropic potential vorticity maps. *Quart. J. Roy. Meteor. Soc.,* **111,** 877–946.
Kimoto, M., H. Mukougawa, and S. Yoden, 1992: Medium-range forecast skill variation and blocking transition: A case study. *Mon. Wea. Rev.,* **120,** 1616–1627.
Konrad, C. E., II, and S. J. Colucci, 1988: Synoptic climatology of large-scale circulation changes during explosive cyclogenesis. *Mon. Wea. Rev.,* **116,** 1431–1443.
Kushnir, Y., 1987: Retrograding wintertime low-frequency disturbances over the North Pacific Ocean. *J. Atmos. Sci.,* **44,** 2727–2742.
Lejenäs, H., and H. Okland, 1983: Characteristics of Northern Hemisphere blocking as determined from a long-time series of observational data. *Tellus,* **35A,** 350–362.
——, and R. A. Madden, 1992: Traveling planetary-scale waves and blocking. *Mon. Wea. Rev.,* **120,** 2821–2830.
Li, Z., and L. Ji, 1997: Efficient forcing and teleconnection patterns. *Quart. J. Roy. Meteor. Soc.,* **123,** 2401–2423.
Liu, Q., 1994: On the definition and persistence of blocking. *Tellus,* **46A,** 286–298.
——, and J. D. Opsteegh, 1995: Interannual and decadal variations of blocking activity in a quasi-geostrophic model. *Tellus,* **47A,** 941–954.
Lorenz, E., 1965: A study on the predictability of a 28-variable atmospheric model. *Tellus,* **17,** 321–333.
Michelangeli, P.-A., and R. Vautard, 1998: The dynamics of Euro-Atlantic blocking onsets. *Quart. J. Roy. Meteor. Soc.,* **124,** 1045–1070.
Nakamura, H., 1994: Rotational evolution of potential vorticity associated with a strong blocking flow configuration over Europe. *Geophys. Res. Lett.,* **21,** 2003–2006.
——, and J. M. Wallace, 1990: Observed changes in the activity of baroclinic waves and their feedback during the life cycle of low-frequency circulation anomalies. *J. Atmos. Sci.,* **47,** 1100–1116.
——, and ——, 1993: Synoptic behavior of baroclinic eddies during the blocking onset. *Mon. Wea. Rev.,* **121,** 1892–1903.
——, M. Nakamura, and J. L. Anderson, 1997: The role of high- and low frequency dynamics in blocking formation. *Mon. Wea. Rev.,* **125,** 2074–2093.
Oortwijn, J., 1998: Predictability of the onset of blocking and strong zonal flow regimes. *J. Atmos. Sci.,* **55,** 973–994.
——, and J. Barkmeijer, 1995: Perturbations that optimally trigger weather regimes. *J. Atmos. Sci.,* **52,** 3932–3944.
Plaut, G., and R. Vautard, 1994: Spells of low-frequency oscillations and weather regimes in the Northern Hemisphere. *J. Atmos. Sci.,* **51,** 210–236.
Pondeca, M. S., A. Barcilon, and X. Zou, 1998a: An adjoint sensitivity study of the efficacy of modal and nonmodal perturbations in causing model block. *J. Atmos. Sci.,* **55,** 2095–2118.
——, ——, and ——, 1998b: The role of wave breaking, linear instability and PV transport in model block onset. *J. Atmos. Sci.,* **55,** 2852–2873.
Rabier, F., E. Klinker, P. Courtier, and A. Hollingsworth, 1996: Sensitivity of forecast errors to initial conditions. *Quart. J. Roy. Meteor. Soc.,* **122,** 121–150.
Rex, D. F., 1950: Blocking action in the middle troposphere and its effect upon regional climate. Part II: The climatology of blocking action. *Tellus,* **2,** 275–301.
Sardeshmukh, P. D., and B. J. Hoskins, 1988: On the generation of global rotational flow by steady idealized tropical divergence. *J. Atmos. Sci.,* **45,** 1228–1251.
Shutts, G. J., 1986: A case study of eddy forcing during an Atlantic blocking episode. *Advances in Geophysics: Anomalous Atmospheric Flows and Blocking,* R. Benzi and A. C. Wiin-Nielsen, Eds., Vol. 29, Academic Press, 135–162.
Simmons, A. J., 1982: The forcing of stationary wave motion by tropic diabatic heating. *Quart J. Roy. Meteor. Soc.,* **108,** 503–534.
——, J. M. Wallace, and G. W. Branstator, 1983: Barotropic wave propagation, instability, and atmospheric teleconnection patterns. *J. Atmos. Sci.,* **40,** 1363–1392.
Talagrand, O., and P. Courtier, 1987: Variational assimilation of meteorological observations with the adjoint vorticity equation. Part I: Theory. *Quart J. Roy. Meteor. Soc.,* **113,** 1311–1328.
Tibaldi, S., and F. Molteni, 1990: On the operational predictability of blocking. *Tellus,* **42A,** 343–365.
——, E. Tosi, A. Navarra, and L. Pedulli, 1994: Northern and South-

ern Hemisphere seasonal variability of blocking frequency and predictability. *Mon. Wea. Rev.,* **122,** 1971–2003.

Tsou, C.-H., and P. J. Smith, 1990: The role of synoptic/planetary scale interactions during the development of a blocking anticyclone. *Tellus,* **42A,** 174–193.

Zeng, Q.-C., 1983: The evolution of a Rossby-wave packet in a three-dimensional baroclinic atmosphere. *J. Atmos. Sci.,* **40,** 73–86.

Zou, X., A. Barcilon, I. M. Navon, J. Whitaker, and D. G. Cacuci, 1993: An adjoint sensitivity study of blocking in a two-layer isentropic model. *Mon. Wea. Rev.,* **121,** 2833–2857.